NERC Scientific Facilities and Technology Ion Microprobe Facility
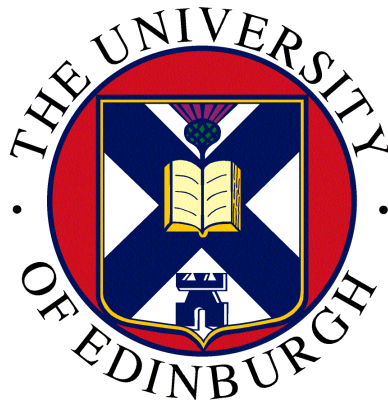
**University Of Edinburgh
NERC Ion Microprobe Facility**

2008 Annual Science Report

<div align="right">

Ion Microprobe Facility
School of Geosciences
Kings Buildings
West Mains Road
Edinburgh
EH9 3JW

</div>

http://www.geos.ed.ac.uk/facilities

Contents

Ion Microprobe Projects (2008)

No.	Name	Report Title
1	K. von Allmen, Th. F. Nägler, Th. Pettke, E. Griesshabe, A. Logan, E. Samankassou	High-resolution $\delta^{18}O$ analyses of two recent brachiopod shells
2	M. Anand & I. J. Parkinson	Variations in Lithium and Boron isotopes in Martian pyroxenes: roles of degassing and diffusion
3	I.S. Buick, S. Kasemann, J. Hermann, M. Satish-Kumar, A. Acosta-Vigil & B. Cesare	The Extent of Lithium Isotope Kinetic Fractionation during Crustal Anatexis
4	Peter Cox, Dr Rachel Wood	Diagenesis vs. oil charge within a carbonate reservoir
5	M. Cusack & P. Dalbeck	Assessing the influence of biological control and low level diagenetic alteration on coral seawater temperature proxies
6	Mascha Dedert, Kate Darling & Dick Kroon	Calcareous nannoplankton productivity during ETM2 (ODP Site 690)
7	I.J. Fairchild	Annual sulphate cycles in an Alpine speleothem: winter temperature proxy
8	L. Field &J. Blundy	The magmatic evolution of Dabbahu Volcano, Afar Rift, Ethiopia
9	N. Hanson, C. Wurster & C. Todd	Atlantic salmon (Salmo salar) otolith thermometry
10	M.C.S. Humphreys	Decompression crystallisation vs mafic injection at the Soufrière Hills Volcano, Montserrat
11	K.Joy & R.Burgess	U-Pb Chronology of Lunar Meteorite NWA 4472
12	A-L. Jourdan, B. Kaeser, & A. Kalt	A light element isotope perspective on the Earth's mantle
13	N. A. Kamenos	Using $\delta^{18}O$ in maerl as both a salinity and temperature proxy
14	A.I.S. Kemp	Proterozoic crustal evolution of the Northern Australian Craton from oxygen and hafnium isotope systematics of detrital zircons
15	C.S.Lane & S.P.E. Blockley	Geochemical variation and characterisation of fine-grained volcanic ash
16	E. Melekhova & J. Blundy	Trace element and volatile evolution in deep crustal hot zones: An experimental case study of primitive basalts from St. Vincent
17	Philip Pogge von Strandmann and Tim Elliott	Li isotope determination of cooling rates
18	D.M. Pyle, S.J.Collins & J. Maclennan	The melt inclusion record of magma storage and degassing at Piton de la Fournaise, Reunion Island
19	K. Vala Ragnarsdottir and Dana Kapitulčinová	Cyanobacterial weathering of minerals
20	A. Ridgwell & D. Schmidt	Ocean acidification during the Palaeogene hydrothermals

21	V.C. Smith, P. Shane & I.A. Nairn	The evolution of the caldera-forming Rotoiti magma, New Zealand, revealed by plagioclase zoning and melt inclusions
22	N.A. Starkey & R.M. Ellam	Melt inclusion compositions of high ^{3}He/^{4}He picrites from Baffin Island and West Greenland
23	C.D. Storey and C.J. Hawkesworth	Probing the birth and growth of continents via isotopic records in titanite
24	R.J.M. Taylor, S.L. Harley, R.W. Hinton & S. Elphick	Distribution of trace elements between zircon, garnet and melt: a key to understanding crustal events and processes
25	E.L. Tomlinson	A snapshot of mantle metasomatism
26	G. Turner, S.A. Crowther & J.D. Gilmour	Plutonium Geochemistry of Meteorites
27	M. Walter, S. Keshav, G. Gudfinnsson, L. Armstrong, J. Tuff, and G. Bulanova	Mineral/melt partitioning of trace elements between carbonate melt and deep mantle phases: constraints on the origin of ultra-deep mineral inclusions in diamonds

High-resolution δ^{18}O analyses of two recent brachiopod shells

K. von Allmen[1], Th. F. Nägler[2], Th. Pettke[2], E. Griesshaber[3], A. Logan[4], E. Samankassou[1,5]

[1]Department of Geosciences, University of Fribourg, Switzerland
[2]Institute of Geological Science, University of Bern, Switzerland
[3]Department of Earth- and Environmental Sciences, Ludwig-Maximilian University Munich, Germany
[4]Department of Physical Sciences and Centre for Coastal Studies, University of New Brunswick, Canada
[5]Department of Geology and Paleontology, University of Geneva, Switzerland

Overview

There are ongoing debates whether brachiopods precipitate their low Mg shells in isotopic equilibrium with ambient seawater or not. The complicated microstructure of a brachiopod shell indicates that there is a strong biological influence (vital effects) on shell secretion. However, many brachiopod species are found to be in or close to isotopic equilibrium with seawater and hence record the ambient seawater temperature in the δ^{18}O composition of their shell.

This study investigates oxygen isotopes in two recent calcite brachiopod shells a) *Terebratulina septentrionalis* (ambient seawater temperature range 7.1°, salinity 30.91-32.14ppt, two-layered shell), and b) *Gryphus vitreus* (quasi-constant seawater temperature and salinity, three-layered shell), in the quest for recorded seasonal temperature signals and signatures of biological control. Measurements were carried out on the Cameca ims-1270 at the NERC Ion Microprobe Facility. External reproducibility is better than 0.50‰, internal uncertainty is better than 0.20‰ (1σ).

Results and Discussion

The SIMS pits have not yet been checked with the SEM for cracks or organic matter that will influence the results. Therefore the results discussed below may be biased and may overestimate the true isotopic range. The δ^{18}O of the ambient seawater was calculated from salinity [1]. δ^{18}O-derived seawater temperatures were calculated using the Epstein et al. formula [2]. SIMS analyses were carried out on 200 μm thick sections cut along the growth direction of the pedicle valves. The remaining halves of the shells were used for GasBench analyses. Pieces of shell of a 1.5 by 3-4mm surface were sectioned along the growth direction. The thin primary layer was not removed explicitly. The secondary layer of *G. vitreus* is only a few micrometers thick and hence the thick tertiary layer was used for SIMS temperature calculations. The oxygen isotopic SIMS range within that tertiary layer of *G. vitreus* is 1.08‰ at maximum per depth profile whereas the total range of all pits is 1.37‰ (Table 1). It has to be pointed out, that the depth profiles (n=3) were concentrated in an older mid-shell area, where apparent growth lines are visible in the tertiary layer. Each depth profile contains between 12 and 17 pits. The average of all tertiary layer data points is 2.03‰. This value is close to the average of the GasBench samples of 2.26‰ (range 0.38‰, average long-term precision is 0.061‰, 1σ). SIMS analyses revealed no isotopic difference between inner and outer secondary layer of *G. vitreus*. The GasBench δ^{18}O-derived average seawater temperature of 13.7°C agrees rather well with the 13.2°C measured on site. The SIMS δ^{18}O-derived average seawater temperature is 1.5° too high at 14.7°C. It might be worth some consideration to apply a small matrix effect correction to the δ^{18}O SIMS data in order to match GasBench results. Matrix effects are discussed in the following column. If all tertiary layer SIMS pits are considered then the total calculated seawater temperature range is 6.2°C. This obviously overestimates the actual temperature range of 0.8°C. However, the external SIMS reproducibility of 0.50‰ can explain a good part of it. Furthermore minor vital effects cannot be excluded.

The five accomplished SIMS depth profiles in *T. septentrionalis* consist of only 5 to 8 pits, as this shell is considerably thinner than the *G. vitreus* shell. Two depth profiles have an intriguingly negative excursion half way through the secondary layer. These excursions will have to be checked with the SEM. The oxygen isotope SIMS range of *T. septentrionalis* is more than four times the range of *G. vitreus* (Table 1). This mirrors nicely the difference between a variable temperature and salinity habitat (*T. septentrionalis*) versus a near–constant temperature and salinity habitat (*G. vitreus*). The *T. septentrionalis* SIMS average of all pits of -1.63‰ is opposed to the 0.87‰ (±0.13‰, 1σ) Gasbench

4

average. Matrix effects very likely cause this offset as *T. septentrionalis* is more enriched in elements than *G. vitreus* (personal communication J. Craven 2008). Therefore all reported *T. septentrionalis* SIMS results were increased by 2.50‰ so that the average of both methods is equal. As opposed to *G. vitreus* and in accordance with literature [3] the oxygen isotopes of *T. septentrionalis* in the outer secondary layer are mostly lighter than in the inner secondary layer where they are close to or in equilibrium with seawater. Therefore we calculated the isotopic range and average of *T. septentrionalis* by only taking into account the 3 innermost GasBench corrected SIMS pit results from each depth profile. The resulting average δ^{18}O-derived seawater temperature is 6.5° which is only 0.6°C below the on-site measured temperature. The calculated innermost secondary layer temperature range of 10.4° is opposed to on site measured range of 7.1°(temperature average and range when using all data points are given in Table 1). This difference could indicate the presence of some vital effects. However, the external reproducibility can also account for a larger calculated temperature range.

Conclusion

To conclude, average oxygen isotopic SIMS data in the center part of a longitudinally cut shell of the low matrix tertiary layer of *G. vitreus* agree quite well with GasBench results but slightly overestimate average ambient seawater temperatures by 1.5°. No metabolic or kinetic trends were discerned throughout the depth profiles, i.e. no enrichment of light isotopes was detected in the outer tertiary layer. This is opposed to findings of *T. septentrionalis* where GasBench corrected average δ^{18}O SIMS results of the inner secondary layer of *T. septentrionalis* are mostly within equilibrium with seawater whereas the outer secondary layer is not. The inner secondary layer of *T. septentrionalis* recorded the whole seasonal temperature range but overestimates it by 3.3°C. High-resolution δ^{18}O SIMS analyses in brachiopod shells may have the potential to detect past changes in climate seasonality. The SIMS method can also help to recognize shells from constant temperature and salinity habitats by revealing the absence of a negative isotopic trend in the outer part of the shell if this characteristic should prove to be present in other brachiopod specimen and species. Average seawater temperatures may be registered in such shells as is the case with *G. vitreus* but seasonal temperature variations will most likely be overestimated. In order to apply the SIMS method to matrix-rich brachiopod samples, crosschecks with the GasBench method are necessary.

Table 1	*G. vitreus* tertiary layer SIMS	all layers GasBench	*T. septentrionalis* secondary layer SIMS	all layers GasBench
SIMS: number of depth profiles	3	-	5	-
GasBench: number of samples along transect	-	16	-	7
δ^{18}O range in ‰	1.37	0.38	6.19	0.50
δ^{18}O average in ‰	2.03	2.26	[a]0.87	0.87
on-site average seawater temp. in °(C)	13.2	13.2	7.1	7.1
δ^{18}O-derived average seawater temp. in °(C)	14.7	13.7	[a]9.0	8.7
" , 3 inntermost pits only	-	-	[a]6.5	-
on-site seawater temp. range in °(C)	0.8	0.8	7.1	7.1
δ^{18}O-derived seawater temp. range in °(C)	6.2	2.2	25.2	3.7
" , 3 inntermost pits only	-	-	10.4	-
[a]*T. septentrionalis* δ^{18}O SIMS results are shifted by +2.50‰ to match GasBench results				

References
[1] Spero, H. J., and D. W. Lea (1996) Marine Micropaleontology, 28, 231-246.
[2] Epstein, S., R. Buchsbaum, H. A. Lowenstam, and H. C. Urey (1953) Geological Society of America Bulletin, 64, 1315-1326.
[3] Auclair, A.-C., M. M. Joachimski, and C. Lécuyer (2003) Chemical Geology, 202, 59-78

The Extent of Lithium Isotope Kinetic Fractionation during Crustal Anatexis

I.S. Buick[1], S. Kasemann[2], J. Hermann[1], M. Satish-Kumar[3], A. Acosta-Vigil[4] & B. Cesare[5]

[1]Research School of Earth Sciences, The Australian National University, Acton, ACT 0200, Australia
[2] School of GeoSciences, University of Edinburgh, Edinburgh EH9 3JW, UK
[3] Institute of Geosciences, Shizuoka University, Ohya 836-1, Suruga-ku, Shizuoka 422-8529, Japan.
[4] Instituto Andaluz de Ciencias de la Tierra, Consejo Superior de Investigaciones Científicas. 18002 Granada, Spain.
[5] Dipartimento di Geoscienze, Universita' di Padova Via Giotto,1, I-35137 Padova, Italy

Introduction

SIMS-based investigations of mantle rocks or mantle-derived melts have shown that, at temperatures in excess of 1000˚C, extreme (15-25‰) intra-grain kinetic fractionation of δ^7Li may occur as a result of the relaxation of lithium concentration gradients and the different diffusivities of ^6Li and ^7Li. As a result, kinetic fractionation of δ^7Li in minerals such as orthopyroxene, clinopyroxene and olivine may render them unsuitable as isotopic tracers. Compared to mantle-derived minerals, there are few SIMS δ^7Li data from minerals in metasedimentary rocks, and it is unclear whether kinetic Li-isotopic fractionation is a problem at temperatures relevant to high-grade metamorphism and anatexis e.g. 650-900˚C. As a result, this study sought to continue work begun in 2007, to assess the extent of kinetic fractionation during crustal anatexis. Samples from two localities were studied: a) a restitic metapelitic granulite in contact with leucogranite (Kerala, Southern India); b) xenocrystal cordierite from a peraluminous dacite from the El Hoyazo in the Spanish Neogene Province.

Results

The Indian restitic sample was chosen to examine the effects of Li diffusion into cordierite and garnet during changing mineral-melt partitioning as a result of crystallisation, a situation known to cause gross Li-isotope disequilibrium in mafic volcanic rocks. A single grain each of garnet and cordierite from the restitic layer was analysed for [Li] and δ^7Li directly at the contact with a leucogranitic layer. Samples from this locality experienced temperatures in excess of 900˚C. The garnet and cordierite are Li-poor (the latter since it forms cm-diameter plates that replaces garnet; Fig. 1a). $[Li]_{Crd}$ increases from ~6 to 10 ppm over 1700 µm toward the leucogranite contact, whereas $[Li]_{Grt}$ is uniformly low (4-5 ppm; data from LA-ICP-MS, ANU) over a ~ 1000 µm traverse. In contrast, plagioclase in the leucogranite has $[Li]_{Pl}$ = 35-45 ppm. With increasing distance into the cordierite, δ^7Li_{Crd} values exhibit a steep trough from +5‰ at the leucogranite contact, to values as low as -7‰ 100 µm inboard (Fig. 1a). At distances greater than 130 µm the cordierite shows intermediate values (0‰ to +3‰) with no systematic zoning pattern (Fig. 1). In contrast, garnet in contact with the leucogranite shows no systematic variation in δ^7Li as a function of distance (Fig. 1b), except for a slightly lower value 35 µm from the leucogranite contact.

The second example involved xenocrystal cordierite (Fig. 2a) within a peraluminous dacite. The cordierite is derived from enclaves of glass-bearing granulite-facies metapelite. Cordierite from one-such enclave was analysed for Li isotopes in 2007; it is shows no consistent zonation in, and a narrow range of, δ^7Li (-7.5±0.9 ‰ to -4.6±1.1 ‰). Xenocrystal cordierite ([Li] = 180-195 ppm) in the dacite has similar δ^7Li despite being in a glassy matrix that contains much lower [Li] contents (~45-50 ppm). Experimental Li partitioning experiments favour glass over cordierite by a factor of 3-10 at 700-850˚C; hence the xenocrystal cordierite is clearly out of trace element equilibrium with the host dacite. Despite this, the xenocrystal cordierite shows little systematic zoning as a function of distance from the dacite (Fig. 2b) margin, and the range of δ^7Li_{Crd} is similar to that of cordierite in the enclaves.

Discussion

Li elemental partitioning in anatectic rocks favours typically cordierite over feldspars. The Li elemental partitioning between cordierite and feldspar at the restite/leucogranite contact reflects disequilibrium. The trough-shaped lowering of δ^7Li_{Crd} within 100 µm of the leucogranite contact is

similar to that predicted from incipient, kinetically-driven Li-isotope fractionation, and is consistent with the increase in $[Li]_{Crd}$ towards the leucogranite contact.
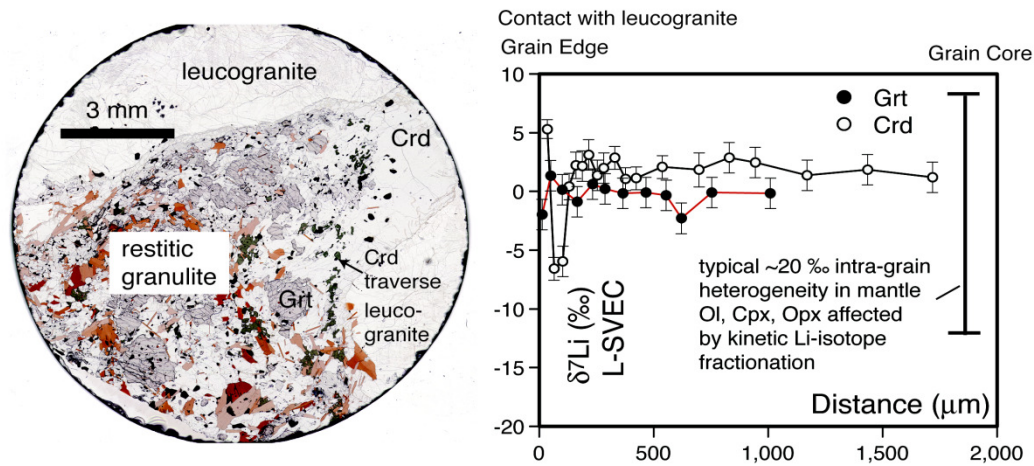
Fig. 1 δ^7Li profile into Li-poor cordierite and garnet in granulite-facies restite in contact with Li-rich leucogranite (error bars = 2σ) from Kerala (Southern India). Scale bar shows the typical magnitude of within-grain heterogeneity typical in studies of mantle materials affected by kinetic Li-isotope fractionation. The cordierite appears to show an incipient diffusion-driven kinetic Li-isotope fractionation within 100 microns of the leucogranite contact, whereas the garnet does not.

In contrast, the garnet grain shows low [Li] and no consistent zonation in δ^7Li, suggesting that it is unaffected by Li diffusion, even though the sample was regionally metamorphosed to temperatures in excess of 900˚C and chosen to maximize the possibility for Li diffusion.
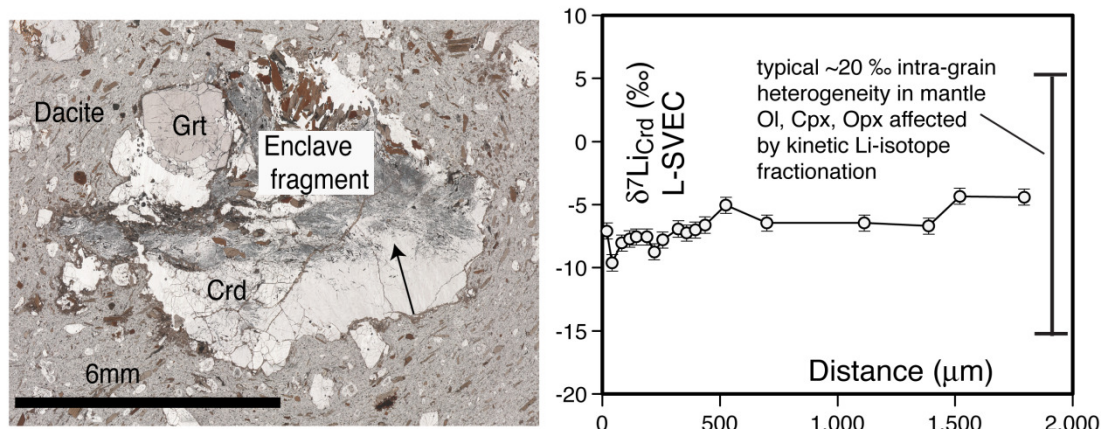
Fig. 2. δ^7Li profile (distance increases in the direction of arrow) into xenocrystal cordierite (error bars = 2σ) in peraluminous dacite (El Hoyazo, Spain). Scale bar shows the typical magnitude of intra-grain heterogeneity typical in studies of mantle materials affected by kinetic Li-isotope fractionation.

Compared with mantle samples, the new data suggest that, at the temperatures relevant to anatexis in the continental crust, minerals such as cordierite and garnet are generally unaffected by kinetic Li isotope fractionation. The robustness of garnet, in particular, is consistent with the requirement that slowly diffusing R^{3+} cations (e.g. Y, REE) are involved in charge-balanced substitutions that introduce Li.

Assessing the influence of biological control and low level diagenetic alteration on coral seawater temperature proxies

M. Cusack & P. Dalbeck

Department of Geographical & Earth Sciences, University of Glasgow
Glasgow G12 8QQ, UK

Introduction

The value of annually-banded reef-building corals as recorders of climate information is well established. Such biological carbonates are produced under exquisite biological control that determines mineral type, polymorph, structure and crystallography. This biological control can complicate the recording of environmental data. To ensure accurate interpretation of seawater temperature, it is imperative to gain a detailed understanding of how biological control influences environmental information. Equally important is our understanding of diagenetic alteration. Since diagenesis alters chemistry and isotopic composition, the detection of even low levels of diagenetic alteration and the knowledge of those regions of coral ultrastructure that are most susceptible to diagenetic alteration, will greatly improve climate interpretations via proxies in corals.

This project used the NERC Ion Probe facility to measure stable oxygen isotope ($\delta^{18}O$) and Sr composition of modern and fossil *Porites* corals. At similar spatial resolution, these measurements were supplemented by electron backscatter diffraction (EBSD) and Atomic Force Microscopy (AFM) at the University of Glasgow. Traditional mass spectrometry measurements were conducted at SUERC and used to determine the offset of the SIMS ^{18}O measurements due to SIMS matrix effects.

Previous analyses of these corals demonstrated the suitability of EBSD as a means of identifying secondary material in corals with the calcite composition of secondary 'dissepiments' and secondary aragonite being readily identified [1]. This project measured the composition of secondary calcite, aragonite fibres and centres of calcification (COC) in fossil *Porites* as well as aragonite fibres and COC in modern *Porites*.
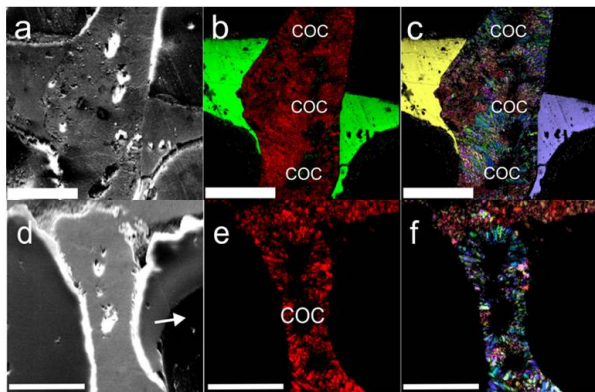
Fig.1 Electron backscatter (EBSD) analysis of horizontal structures in fossil (top a-c) and modern (bottom d-f) coral. Secondary electron images (a, d) of the areas analysed by EBSD. Phase maps (b, e) of the regions in a and d, present aragonite as red and calcite as green. Crystallographic orientation maps (c, f) of the same regions indicate the crystallographic orientation of aragonite. Scale bars = 50 μm (top) 60 μm (bottom).

The specific objectives of the project were to determine:
- Variation in Sr/Ca and $\delta^{18}O$ between and within parts of the modern coral skeleton.
- Whether the original dissepiments differ from the fasculi in Sr/Ca or $\delta^{18}O$
- Differences in Sr/Ca and $\delta^{18}O$ between original and secondary dissepiments and the influence on seawater temperature calculations

All of these objectives have been met and are presented in summary in Figures 2 & 3.

Results

The secondary calcite is isotopically lighter than both fossil and modern aragonite (Figure 2). The oxygen isotope composition of both fossil and modern corals were compared with a known value for two other corals studied in this area [2], and were also compared with conventional mass spectrometry

values to account for SIMS matrix effects. This brought the aragonite signatures in both specimens to within expected values. However, the calcite in the fossil specimen still revealed significant offset.
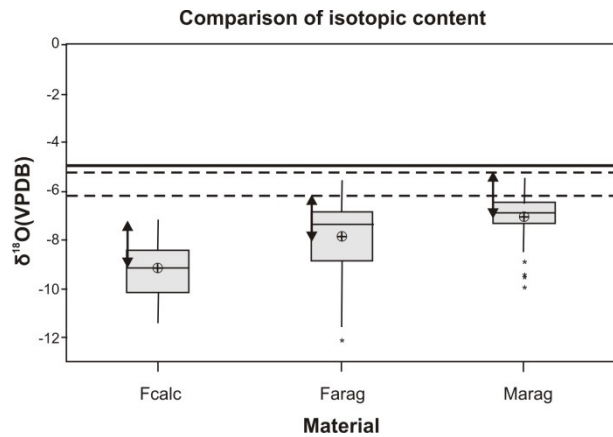
Fig. 2 Boxplots of stable oxygen isotope composition of modern coral aragonite and fossil coral aragonite and calcite as determined by Secondary Ion Mass Spectrometry (SIMS). The solid horizontal line represents the mean $\delta^{18}O$ values for the modern and fossil coral obtained via conventional mass spectrometry. The double arrow indicates the offset required to adjust the mean SIMS values for modern coral aragonite to coincide with mean conventional values. The dashed horizontal lines represents mean $\delta^{18}O$ values obtained for two modern corals from previous publications in the area of study [2].

Trace element composition of both modern and fossil *Porites* coral using the Cameca 4f revealed differences between the calcite and aragonite in the fossil specimen as well as differences between the main skeletal aragonite and the COCs. Secondary calcite has the lowest and most varied strontium content (Figure 3). In summary, Sr/Ca ratios of secondary calcite result in calculated sea surface temperatures (SST) much reduced from reality while fossil COC Sr/Ca would generate somewhat elevated calculated temperatures while fossil aragonite fibres and modern fibres and COC result in calculated temperatures that fall within the actual temperature range (Figure 3)
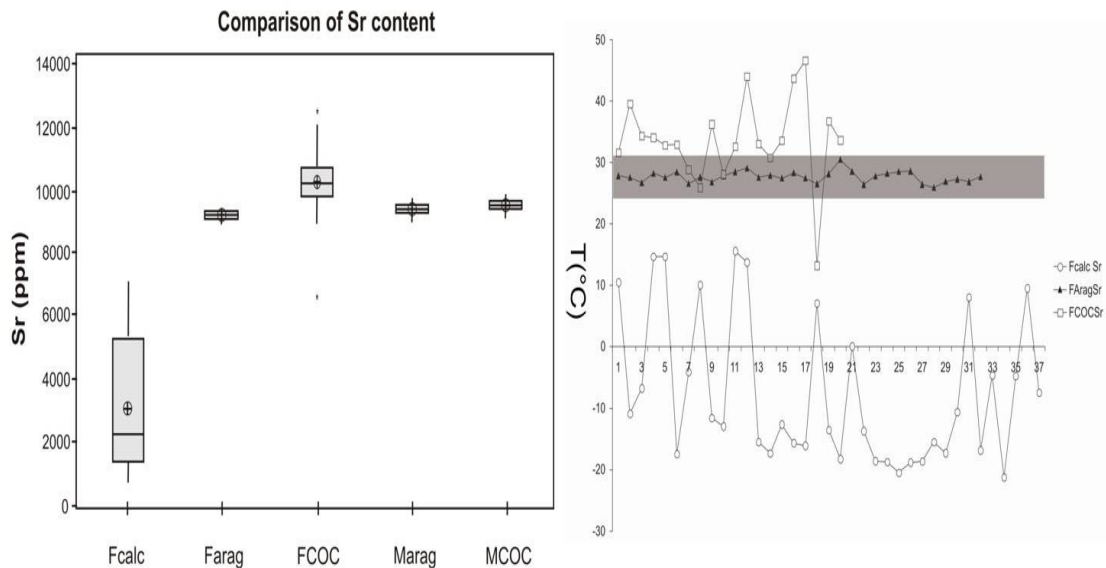
Fig. 3 Left: Strontium concentration in fossil coral calcite (FCalc), aragonite (FArag) and COC (FCOC) and modern coral aragonite (MArag) and COC (MCOC). Right: Calculated water temperature based on strontium concentration in fossil coral with actual temperature range for the sample collection region represented by the grey region.

Conclusions

The distinct differences in composition between secondary calcite material and primary aragonite in both the fossil and modern specimens underlines the importance of careful sample screening of coral material prior to analysis [3, 4, 1, 5]. The secondary calcite in this study mimics morphological structures of the original aragonite skeletal material yet yields distinct anomalies in geochemistry that result in large offsets in calculated SST. Thus, deliberate steps are required to avoid inclusion of such material in SST calculations, ensuring that only pristine, original material is selected for climate proxy studies.

References
[1] Cusack, M., et al., 2008. *Coral Reefs*. **27**, 905-911.

[2] McCulloch, M.T., et al., 1999. *Science*. **283**, 202-204.
[3] Allison, N., et al., 2005. *Geochimica et Cosmochimica Acta*. **69**, 3801-3811.
[4] Allison, N., et al., 2007. *Geochimica et Cosmochimica Acta*. **71**, 4693-4703.
[5] Nothdurft, L.D., et al., 2007. *Geochimica et Cosmochimica Acta*. **71**, 5423-5438.

Annual sulphate cycles in an Alpine speleothem: winter temperature proxy

I.J. Fairchild[1]

[1]School of Geography, Earth and Environmental Sciences, University of Birmingham, Birmingham B15 2TT

Objectives

This work formed part of a NERC standard grant *Atmospheric Forcing of Sulphate in Speleothem Carbonate* which aimed to exploit the discovery [1] of the preservation of a modified 20th century atmospheric S pollution signal in cave carbonate deposits (speleothems), where the S is present as sulphate hosted in the calcite lattice. A specific project objective was to clarify the role of pH in the incorporation of sulphate in speleothems and to explore its use in palaeoenvironmental analysis. The ion probe application is to examine an annually-laminated sample from Obir cave in Austria [2] where detailed monitoring and modelling of the carbonate system has demonstrated that seasonal changes in cave ventilation lead to strong changes in the composition of cave air and the pH of dripwaters leading to less sulphate incorporation in winter when pH is high. Through study of around 15 annual layers in earlier ion probe work [3], we have established that annual variations in sulphate exist in this carbonate sample even though dripwaters have seasonally-invariant sulphate compositions. We hypothesize that the annual sulphate profile in the speleothem reflects that of the seasonal temperatures. Long, cold winters should give rise to greater thicknesses of calcite with low sulphate content. Hence the main objective was to obtain a 100-130 year time series of S variations in stalagmite to compare with instrumental records with a secondary objective to examine the range of halogen elements that could be detected.

Results

The long-term record of S was achieved, confirming the presence of annual variations in S through a 120 year period, but the statistical comparison with the climatic data will take some time to work out. Of more immediate interest to readers of this report was the novel identification of significant halogen behaviours as shown in Figure 1 from [3]. Chloride displays a flat distribution whereas F, Br and I follow P in being enhanced in abundance at annual fluorescent laminae (and also some sub-annual laminae in this particular transect).
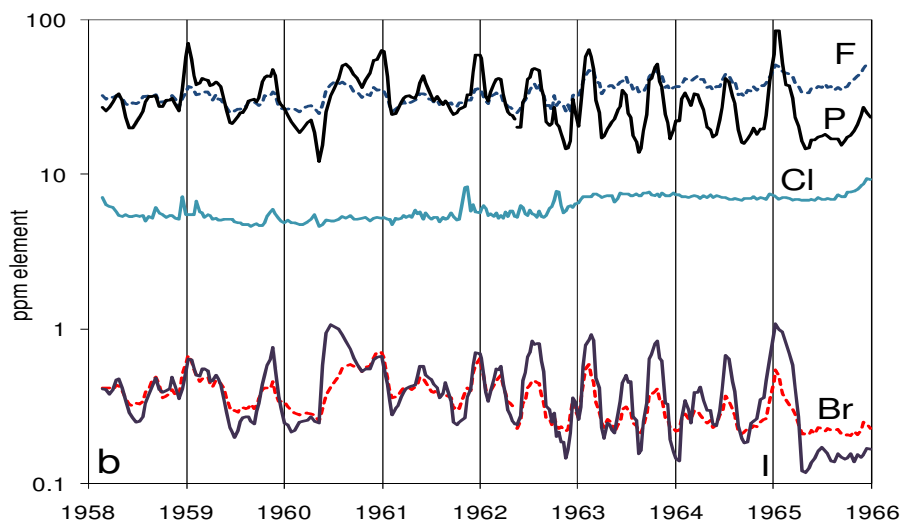
Fig. 1 Chemical trends in sample Obi84 for the years 1958 to 1966. Ion microprobe analysis of negative secondary ions. P, F, Br and I enrichments coincide with visible laminae, but Cl does not display distinctive variation.

References

[1] S. Frisia, A. Borsato, I.J Fairchild, and J. Susini, J. Earth Plan. Sci. Lett. 235 (2005), 729-740.

[2] C. Spötl, I.J. Fairchild and A.F. Tooth (2005) Geochim. Cosmochim. Acta, 69 (1983), 2451-2468.

[3] Fairchild, I.J., Spötl, C., Frisia, S., Borsato, A., Susini, S., Wynn, P.M., Cauzid, J. and EIMF. Petrology and geochemistry of annually laminated stalagmites from an Alpine cave (Obir, Austria): seasonal cave physiology. In:

Pedley, H.M. and Rogerson, M. (eds) *Tufas and speleothems* Geological Society Special Publication (submitted January 2009).

The magmatic evolution of Dabbahu Volcano, Afar Rift, Ethiopia

L. Field[1] & J. Blundy[1]

[1]Dept of Earth Sciences, University of Bristol, Wills Memorial Building, Queen's Road, Bristol BS8 1RJ

Fig.1 View of Dabbahu from the southwest.

Aims and Objectives

The aim of this research is to gain further understanding of magmatic processes occurring in an active continental rift environment. The Dabbahu magmatic centre, in the Afar region of Ethiopia, burst back into life in 2005 with rifting events associated with the emplacement of basaltic dykes; however the only associated erupted magma was rhyolitic. Analysis of melt inclusions in samples collected from Dabbahu will allow reconstruction of the history of the magma, evidencing any dramatic changes in conditions which have occurred. Phenocryst hosted melt inclusions are used to determine the depth-composition-density evolution of the magma. The NERC studentship is allied to a major interdisciplinary study investigating active magmatism and tectonics in the Afar region, Ethiopia. The larger project aims to track the creation, migration, evolution and emplacement of magma from the asthenosphere to the crust. This work builds on the foundations laid by Barberi, et al. [1], with the aim of gaining more of an understanding of pre-eruption processes and their timescales in continental rift related magma chambers.
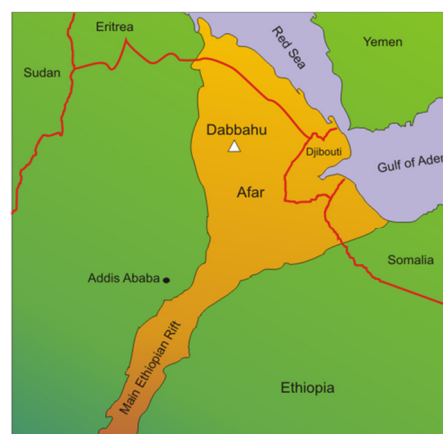
Fig. 2 Map showing location of Dabbahu.

Analysis

Samples were collected from Dabbahu during the Jan/Feb 2008 fieldseason. Analysis in 2008 concentrated on samples from the rhyolitic obsidian flows which dominate the northern half of the volcano. The dominant phenocryst is alkali feldspar (anorthoclase). The lava flows are very young (available age data places the volcano at ~44 kyrs [2]) and therefore the feldspars are very fresh, and ideal for ion microprobe analysis. 100 analyses were carried out on melt inclusions, glasses and the feldspar hosts.

Individual crystals and glass fragments were picked and resin mounted. As ^{12}C was being measured in order to give CO_2 values, the mounts were left uncoated for preliminary SEM work to prevent contamination from the carbon coating.
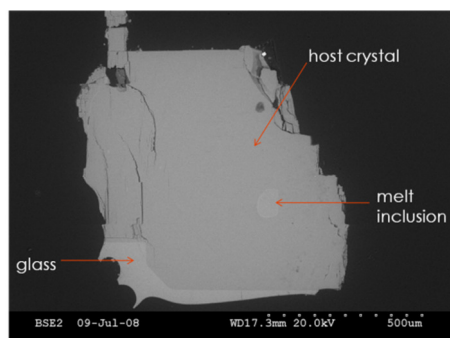
Fig. 3 Backscatter SEM image of a typical melt inclusion and the alkali feldspar host.

EMPA analysis was also carried out after the SIMS analysis. As well as ^{12}C, ^{1}H (to give H_2O values) and a range of trace elements were also measured.

Results

The CO_2 and H_2O values obtained covered a range of values, with the melt inclusions having the highest values, and the pumice and obsidian glass have values at the lower end of the scale, consistent with degassing. The H_2O values obtained ranged from 0.01 – 5.25 wt%. The obsidian and pumice groundmass values range from 0.01 – 2.91 wt %. This is consistent with published data for pantellerites e.g. Greater Olkarra VP - 3.4 wt % [3], Eburru, Kenya, up to 5.6 wt % [4]. CO_2 values obtained range from 0 – 1638 ppm with the obsidian and pumice groundmass values ranging from 0-349 ppm. The low CO_2 and H_2O values obtained from the matrix glasses indicate the lavas and pumices are largely degassed. However, the CO_2 values in these pumices are higher than expected in some instances which suggests some secondary enrichment: in pumices this may be due to an increase in pressure following an explosive eruption phase and subsequent collapse in the conduit; in the obsidians, this may be due to a slight increase in pressure during emplacement of a flow following collapse of the initial permeable foam.

Fig. 4 graph showing CO_2 v H_2O, highlighting the general degassed nature of the pumices and the obsidians.

The CO_2 and H_2O values were input into VolatileCalc [5] in order to gain insights into the depths of melt inclusion entrapment. The initial results indicate a multiple levels of magma storage with a main magma storage area at ~ 5 km depth which corresponds to the modelled mogi source (Tim Wright, Leeds). One melt inclusion indicated an entrapment depth of 13.3 km.

Further work

Further analysis will be carried out in 2009. Further melt inclusions from sample 55 (which yielded the deepest entrapment depth) will be analysed to determine if further evidence of a deeper magma chamber can be found. Phenocrysts from additional samples collected during the 2008 and 2009 field seasons will also be analysed to further contribute to the reconstruction of the magmatic system beneath Dabbahu.
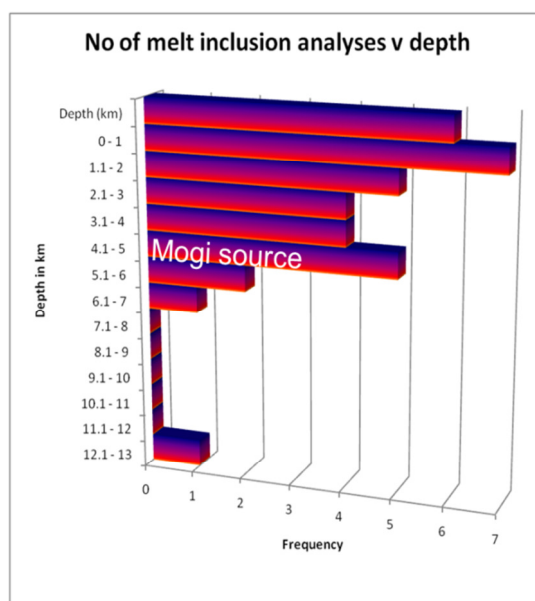
Fig. 5 Graph showing melt inclusion depth of entrapment, and hence inference of magma storage depths.

References

[1] F. Barberi, Journal of Petrology 16(1) (1975) 22-56
[2] F. Barberi et al., Journal of Geology 80(6) (1972) 720-729
[3] M.C. Wilding et al. Contr. To Mineralogy and Petrology 114(2) (1993) 264-275
[4] B. Scaillet & R. Macdonald, Lithos 91(1-4) (2006) 95-108
[5] S. Newman & J.B. Lowenstern, Computers & Geosciences 28(5) 597-604
[6] K. D. Putirka, Minerals, inclusions and volcanic processes: Reviews in Mineralogy and Geochemistry 69, 61-120.

Atlantic salmon (*Salmo salar*) otolith thermometry

N. Hanson[1], C. Wurster[2] & C. Todd[1]

[1]Scottish Oceans Institute, University of St. Andrews, St. Andrews KY16 8LB, UK
[2]School of Geography and Geosciences, University of St. Andrews, St. Andrews KY16 9AL, UK

Background

Long term declines in Atlantic salmon abundance have been linked to reductions in marine survivorship and in particular, reductions in growth condition (a measure of fish quality) have been correlated to rises in mid-winter sea surface temperature anomalies in the Northeast Atlantic (Todd et al. 2008). It was hypothesized that fish returning to Scotland in relatively poor (i.e. underweight) condition may have inhabited warmer waters during their marine residency than those returning in relatively good condition. Direct observations of marine migration and feeding preferences within the North Atlantic are difficult to achieve. However, otoliths ('ear stones') of Atlantic salmon have the potential to provide insight into the thermal regime experienced by the fish during this elusive lifestage. Otoliths are primarily composed of aragonite, a polymorph of calcite ($CaCO_3$). $\delta^{18}O$ values of otolith aragonite are deposited at or near isotopic equilibrium with ambient water, and fractionation between the two is mediated by temperature (e.g. Kalish 1991). Therefore, if the $\delta^{18}O$ value of ambient water is known, the temperature of that water during formation of the otolith can be calculated. This one-day pilot study investigated the use of Secondary-Ion-Mass-Spectrometry (SIMS) for determination of high-resolution otolith $\delta^{18}O$ profiles from a fish returning in relatively good condition and from one returning in relatively poor condition.
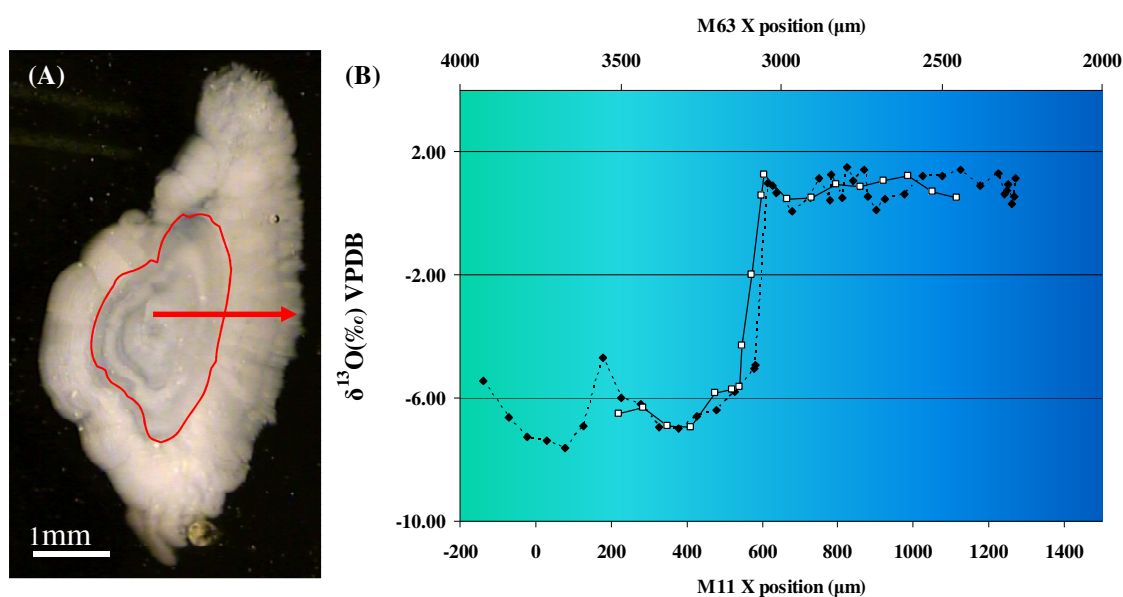
Fig. 1 (A) An example otolith specimen showing direction of transects and the 'transition zone' between freshwater (inner region) and marine (outer region) residency. (B) $\delta^{18}O_{otolith}$ profiles for M11 (black diamonds) and M63 (open circles).

Results & Discussion

We obtained 43 $\delta^{18}O_{otolith}$ measurements from fish M11 (~30% underweight) and 19 measurements from fish M63 (normal condition fish), focusing on a) the transition zone between freshwater and marine residency and b) the outermost region of the otolith corresponding to the most recent growth. There were no significant differences between the two otoliths. Both transects clearly showed a 5-6‰ increase in d18O values between freshwater and marine zones (Figure 1). This transition was also reflected in preliminary micromilled samples from similar otoliths (unpublished data); however, SIMS allowed us to demonstrate that the transition occurs rapidly (within 30μm). Within the marine zone, M11 $\delta^{18}O_{otolith}$ values were slightly more variable (Max = 1.50‰ Min = 0.08‰, Median = 0.90‰, s.d. = ±0.40‰) than M63 $\delta^{18}O_{otolith}$ values (Max = 1.27‰ Min = 0.47‰, Median = 0.79‰, s.d. =

±0.31‰), which may have resulted from different sampling resolutions. However, there were no significant differences between the two (two-sample t-test, p = 0.859).

Several fractionation equations are available for otolith thermometry. All have similar slopes but significantly different intercepts, suggesting that inter-specific variation in otolith precipitation and/or metabolism drives differences in fractionation. While no temperature fractionation equation has yet been developed specifically for salmonids, we are mainly interested in relative difference between individuals rather than the reconstruction of absolute thermal histories. The laboratory-derived equation provided by Kim and O'Neil (1997) developed for synthetic calcite and adapted for aragonite was used to calculate temperature for the two otolith profiles, using an averaged $\delta^{18}O_{seawater}$ value of 0.26‰ (average data over 0-10ºE, 65-75ºN from Schmidt et al. 1999). Calculated temperatures for both fish varied between 10 – 17ºC, within the published thermal tolerance for this species but higher than expected temperature fluctuations within their migration route in the Northeast Atlantic. This overestimation of absolute temperature is likely the result of species specific fractionation relationships but as we are mainly concerned with differences between fish rather than absolute reconstruction of temperature, this equation will be used until a more suitable one is developed. There were no major and consistent differences in temperature profiles between the poor and good condition fish, suggesting that the two share a similar thermal history, although broader conclusions cannot be drawn from these preliminary results.
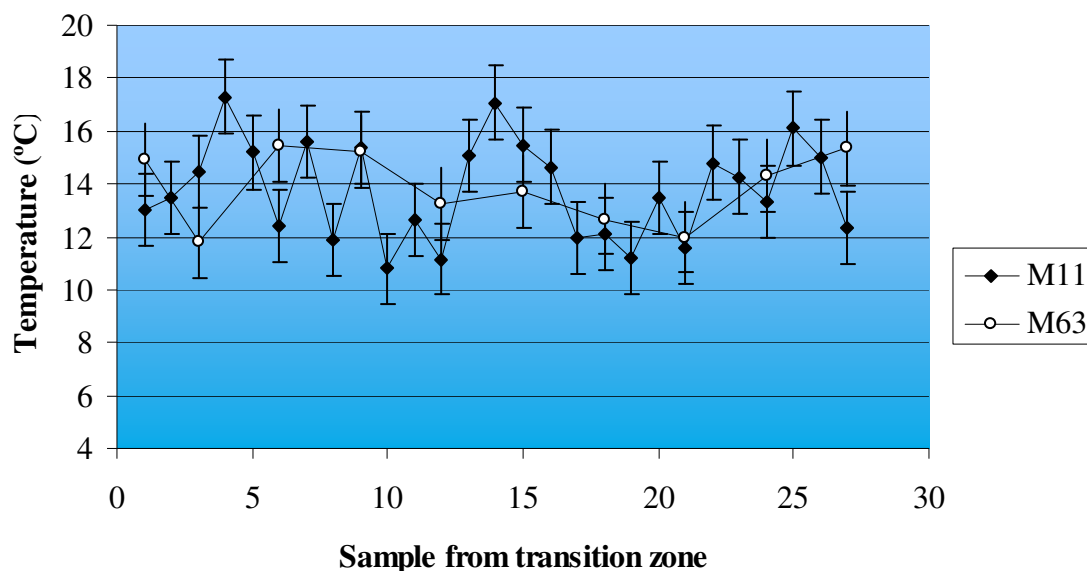
Fig. 2 Thermal histories for a good condition salmon (M63) and a poor condition salmon (M11) calculated from $\delta^{18}O_{otolith}$ values. Error bars represent the upper and lower temperature boundaries given an analytical precision of ±0.30‰ for $\delta^{18}O$ values.

References

[1] C. D. Todd, S.L. Hughes, C. T. Marshall, J.C. MacLean, M.E. Longeran & E.M. Biuw, Global Change Biology 14 (2008) 958-970

[2] J.M. Kalish, Marine Ecology Progress Series 75 (1991) 191-203

[3] S.T. Kim & J.R. O'Neil, Geochimica et Cosmochimica Acta 61 (1997) 3461-3475

[4] G.A. Schmidt, G.R. Bigg & E.J. Rohling, Global Seawater Oxygen-18 Database. (1999) available from: http://data.giss.nasa.gov/o18data/

Decompression crystallisation *vs* mafic injection at the Soufrière Hills Volcano, Montserrat

M.C.S. Humphreys

Department of Earth Sciences, University of Cambridge, Downing Street, Cambridge, CB2 3EQ

Introduction

Many arc magmas show petrological features that indicate an episode of heating shortly prior to eruption (e.g. reverse zoning in Fe-Ti oxides and orthopyroxenes). These petrological features are commonly attributed to mafic magma injection, but the large latent heating effect associated with decompression crystallisation could also be responsible [1]. Dome-forming eruptions, including that at Montserrat, commonly display evidence for both mafic magma recharge (in the form of excess SO_2 gas emissions, mafic inclusions and partially reacted xenocrysts, e.g. [2-4]), and decompression crystallisation [5]. The mafic inclusions disaggregate during ascent and are a major source of microlites in the andesite [4]. Mafic recharge is an important control on eruptive style and could affect the bulk magma composition and viscosity in the chamber, while latent heat release will affect the temperature and thus viscosity of ascending magma. A good understanding of the relative roles of latent heat and mafic magma injection is therefore vital.

Approach

Recent advances in thermobarometry allow temperature to be estimated to within $\pm 20°C$ from plagioclase-glass pairs [1,6]. When combined with the volatile contents of melt inclusions, which provide information about entrapment pressures, magmatic P-T paths can be determined. In this study, H_2O, CO_2, Li and Cl contents of plagioclase-hosted, rhyolitic melt inclusions were measured, together with the host mineral composition, in order to estimate the P-T path of the magma and the degassing mechanism. Incompatible trace elements were also analysed in order to quantify the extent of decompression crystallisation. Pockets of matrix glass from mafic inclusions were compared with the melt inclusions from the andesite, in order to assess the presence of a mafic component.

Results and preliminary interpretations

High volatile contents were recorded in melt inclusions from pumice, with H_2O contents up to 6.2 wt% (equivalent to a pressure of ~ 225 MPa if H_2O-saturated). Melt H_2O contents increase with SiO_2 (calculated on an anhydrous basis) which suggests decompression-driven crystallisation [7]. Calculated temperatures range widely from 820 °C to >950 °C, and increase as H_2O (and pressure) decreases (figure 1).
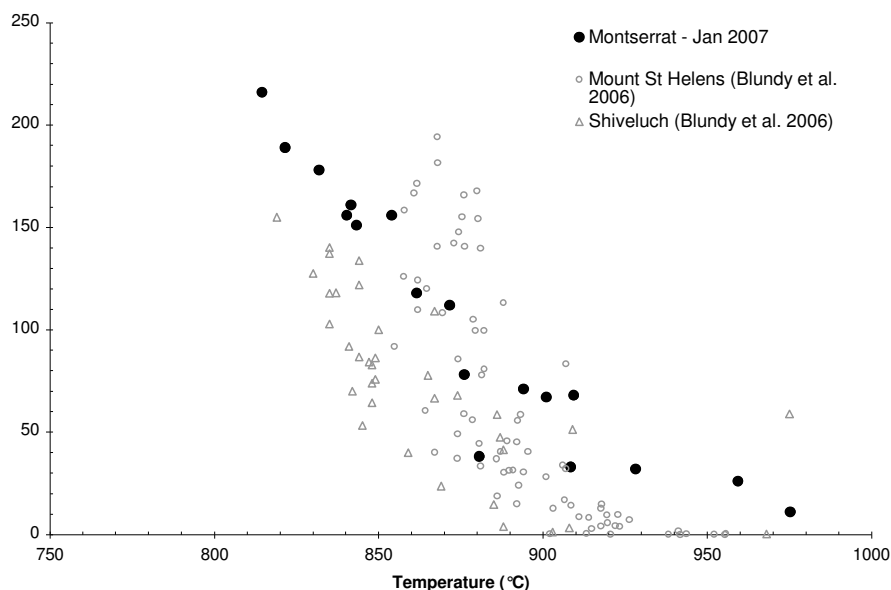
Fig. 1 Variation of plagioclase-liquid temperatures estimated from melt inclusion–host pairs [6] with pH$_2$O.

CO_2 contents appear to be high, indicating a deeper magma source than previously believed. Cl contents are also high, 0.13 to 0.44 wt%. Both Cl and Li correlate with H_2O contents, which suggests that they partition into the vapour during decompression. The co-variation of Cl with H_2O is consistent with either closed-system degassing, or open-system degassing with limited amounts of crystallisation accompanying exsolution. Melt inclusions from dome rocks have very low H_2O concentrations. On the basis of their Cl and CO_2 contents, which are similar to those from pumice, these inclusions have been dehydrated, possibly by diffusion of H^+ out of the inclusions during shallow storage in the dome.

Trace element contents are very scattered and show little clear variation with either $SiO_2(n)$ or H_2O, despite evidence of decompression-driven crystallisation. This suggests that trace element abundances are controlled by another process, perhaps mixing with less evolved (mafic) material during crystallisation. This possibility will be investigated further in the coming months.

References
[1] J. Blundy, K. Cashman, & M. Humphreys, Nature 443 (2006) 76-80.
[2] M. Edmonds, D. Pyle & C. Oppenheimer, EPSL 186 (2001) 159-173.
[3] M.D. Murphy, R.S.J. Sparks, J. Barclay, M.R.Carroll & T.S. Brewer, J Petrol 41 (2000) 21-42
[4] M.C.S. Humphreys, T. Christopher & V. Hards, CMP 157 (2009) 609-624
[5] V.J.E Buckley, R.S.J. Sparks & B.J. Wood, CMP 151 (2006) 121-140
[6] K.D. Putirka, Am Mineral 90 (2005), 336-346
[7] J. Blundy & K. Cashman, Geology 33 (2005) 793-796

U-Pb Chronology of Lunar Meteorite NWA 4472

K.Joy[2,3] & R.Burgess[1]

[1]School of Earth, Atmospheric and Environmental Sciences, Uni. of Manchester, Manchester, M13 9P, UK
[2]The Joint UCL / Birkbeck Research School of Earth Sciences, London, WC1E 6BT, UK
[3]Dept. of Mineralogy, The Natural History Museum London, UK

Introduction

Lunar meteorites provide geological samples of the Moon from regions that were not sampled by the US Apollo and Soviet Union Luna sample return missions. These important samples are providing vital new information about the thermal and magmatic history of the Moon. For example, basaltic and basalt-bearing lunar meteorites have extended the known range of lunar partial melting and volcanism to as long ago as 4.35 Ga and as recently as ~2.8 Ga (previous to this the Apollo and Luna mare basalt samples provided a more restricted view of lava crystallisation ages from ~3.85 to 3.1 Ga [1]).

North West Africa (NWA) 4472 is a heterogeneous lunar meteorite breccia that was collected in Algeria in 2006. The sample comprises a mixture of rock and mineral fragments (Fig. 1a [2]), which were derived from different bedrock environments and were fused together in the lunar regolith (surficial soil-like layer). Part of this clast inventory includes several basaltic rock fragments that originate from several compositionally distinct lava flows and mantle source regions. This study was designed to investigate the crystallisation ages of these basalts, and to relate their chronological and petrological history to the Apollo, Luna and lunar meteorite sample collection [1].
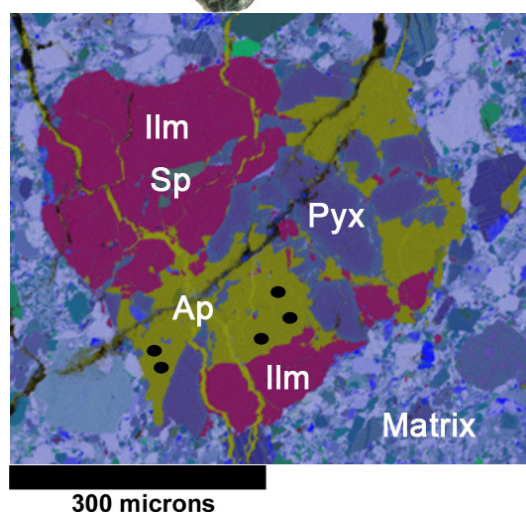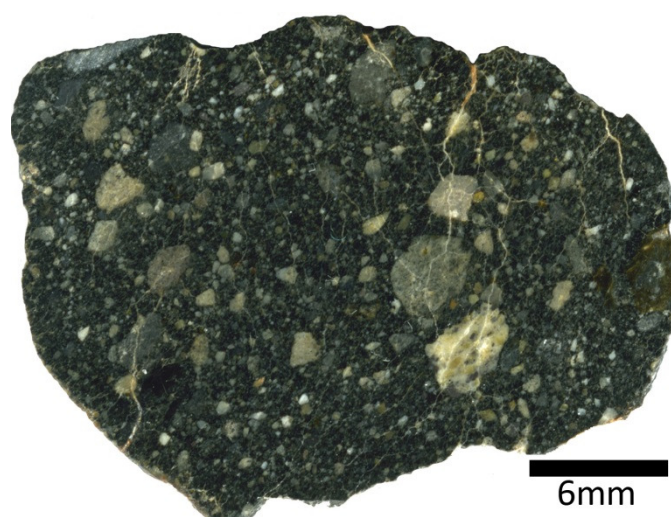
Fig. 1. *Left:* (a) Photograph of a polished surface of the main mass of NWA 4472 illustrating the clast-rich nature of the meteorite. *Right:* (b) False colour X-ray map of a basalt clast (flourapatite-pyroxene-ilmenite assemblage) in NWA 4472 showing individual mineral phases where Ilm = ilmenite, Pyx = pyroxene, Ap =

apatite, Sp = spinel. Colours represent concentration of different element where Si = blue, Al = white, Mg = green, Fe = red, Ca = yellow and Ti = pink. Locations of the ion probe measurements made by this study are denoted by black spots.

Results

U-Pb and Pb-Pb isotope data was obtained from phosphates located in three sub-sections of NWA 4472 [3]. Apatites were analyzed in both discrete mineral grains within the NWA 4472 matrix, and in polymict mare basalt clasts such as the clast shown in Fig. 1b. Results are illustrated in Fig. 2a, are described in [3], and are summarized below:

- Five points analyzed in zoned fluorapatite grains within the basalt clast shown in Fig. 1a yielded an average ^{207}Pb/^{206}Pb age of 3931 ± 18 Ma (2σ) and have a U-Pb concordia age (Fig. 2a: red ellipses) of 3937 ± 18 Ma (2σ).
- Two analyses within a discrete matrix fluorapatite grain gave an average ^{207}Pb/^{206}Pb age of 4345 ± 24 Ma (2σ) and have a U-Pb concordia age (Fig. 2a: green ellipses) of 4344 ± 14 Ma (2σ).
- An analysis of a second matrix apatite grain gave a ^{207}Pb/^{206}Pb age of 4070 ± 18 Ma (2σ) and has a U-Pb concordia age (Fig. 2a: yellow ellipse) of 4070 ± 27 Ma (2σ).
- An analysis within a third matrix fluorapatite grain gave a ^{207}Pb/^{206}Pb age of 3966 ± 12 Ma (2σ) and has a U-Pb concordia age (Fig. 2a: blue ellipse) of 3968 ± 20 Ma (2σ).

The majority of the merrillite grains analyzed in this study were isolated fragments within the NWA 4472 matrix (i.e. they were not associated with any other mineral phase). Two merrillite grains yielded ^{207}Pb/^{206}Pb ages of 3936 ± 22 Ma (2σ) and 3936 ± 18 Ma (2σ), which is consistent with the dates (3.93-3.94 Ga) of apatites within the basalt clast shown in Fig. 1b. Two other merrillite grains gave similar slightly older ^{207}Pb/^{206}Pb ages of 3951 ± 16 Ma (2σ) and 3956 ± 18 Ma (2σ) that cannot be specifically correlated with any of the apatite age dates shown in Fig. 1b.

The data show that lunar phosphate grains can be dated successfully and with high precision using the Edinburgh Cameca ims1270.
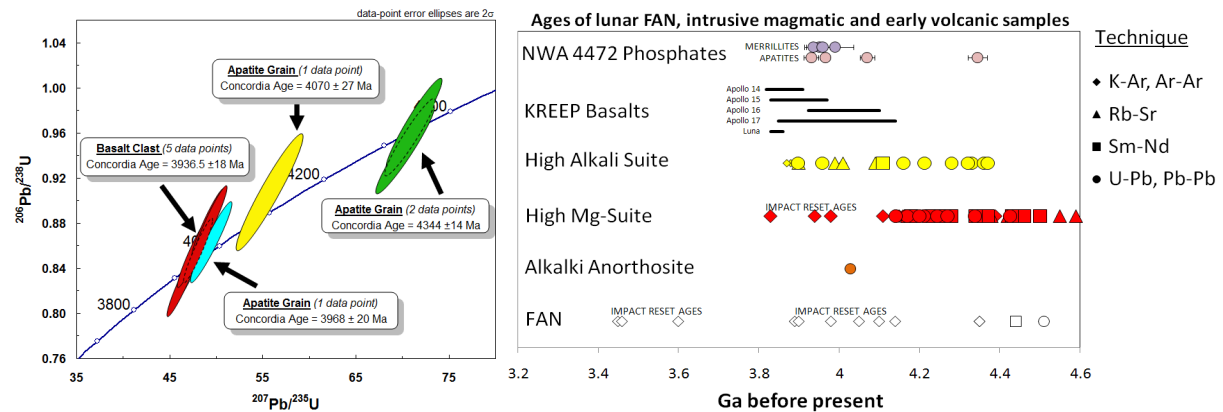
Fig. 2 *Left:* (a) U-Pb concordia plot constructed using Isoplot. Apatite results are shown for the KREEP basalt clast shown in Fig. 1b (red coloured ellipse) and three isolated matrix apatite fragments. Solid ellipses represent analyzed data and dashed ellipses are Isoplot concordia ages. Decay constant errors are included in the error calculation. *Right:* (b) NWA 4472 phosphate crystallization ages dates measured in this study (Pb-Pb ages with 2σ error bars) compared with the literature age dates of lunar crustal rocks (ferroan anorthosite [FAN], High Mg-Suite and High Alkali Suite) and volcanic KREEP basalts [1].

Lunar Science Implications

Results of this study indicate that NWA 4472 has sampled a range of lunar Pre-Nectarian period (>3.92 Ga) lunar volcanic (KREEP basalts) and plutonic lithologies. We interpret that the ages determined by this study to represent the crystallization ages of various lithic components within the NWA 4472 regolith [2, 3]. The evolved mare basalt fragment (Fig. 1b) dated to be 3.93 - 3.94 Ga, and the matrix apatite and merrillite grains (3.94 - 4.07 Ga) are consistent with the ages of Apollo 15, 16 and 17 KREEP (incompatible trace element rich) mare basalts (Fig. 2b). We suggest that the older

apatite grain, dated to be ~4.34 Ga, might represent the crystallization date of a rare granitic (lunar High Alkali Suite) clast component.

It has been proposed [2] that the meteorite probably originated from the nearside of the Moon from an area around the periphery of the large Imbrium impact basin [2]. Therefore the KREEP basalt volcanism dated by this study (>3.93 Ga; Fig. 2 [3]) must have predated the formation of Imbrium (~3.85 Ga) and associated subsequent basin-filling mare basalts (<3.85 Ga). This conclusion has interesting implications for understanding the magmatic history of the Moon.

References

[1] L. E. Nyquist and C. -Y.Shih. GCA. 56 (1992) 2213-2234.

[2] K. H. Joy, I.A. Crawford, A.T. Kearsley, V.A. Fernandes, R. Burgess, A. J. Irving, EIMF. In Lunar and Planetary Science *XXXVIX,* (2008), abstract no. 1132

[3] K. H. Joy, R. Burgess, R. Hinton, V.A. Fernandes, I.A. Crawford, A.T. Kearsley, A. J. Irving, EIMF. In Lunar and Planetary Science XL (2009)*,* abstract no. 1708

[4] K. Terada, Y. Sasaki, M.Anand, K.H. Joy, and Y. Sano. EPSL 259 (2007) 77-84.

A light element isotope perspective on the Earth's mantle

A-L. Jourdan[1], B. Kaeser[1], & A. Kalt[1]

[1]Institut de Géologie, Université de Neuchâtel, 2009 Neuchâtel, Switzerland

Overview of the project

In this study, we aimed at investigating and comparing the light element (Li and B) concentration and isotope characteristics of the mantle in the three global geodynamic settings: the mantle wedge above a subduction zone, the young stable sub-continental mantle, and the reworked subcontinental mantle in a rift context. There is relatively little chemical information available on the light element signature of the mantle itself, and particularly on its isotope composition, other than through the analysis of magmas derived from the partial melting of such a source.

The potential importance of isotope diffusive fractionation requires that any Li (and B) isotopes investigation on mantle xenoliths include in-situ measurement of Li (and B) isotope ratios by SIMS (using the Cameca IMS 4f, Ion Microprobe Facility Edinburgh) to tackle this issue. The project as a whole was designed to contribute to research on the behavior of Li (and B) during crustal recycling and mantle modification processes, through the characterization and understanding of inter-mineral or melt-mineral isotope fractionation and disequilibrium processes.

Background

We have planned to investigate two suites of well-studied mantle xenoliths from the Patagonian plateau (South America) coming from the mantle wedge (Cerro del Fraile Volcanic Field [1]) and from a stable continental root (Pali Aike Volcanic Field [2]), and to extent the work done by B. Kaeser on xenoliths from Marsabit (Africa) representing a mantle reworked in a rift context [3][4] .The three suites of xenoliths have already been carefully and thoroughly described in terms of mineralogy, trace element and radiogenic isotope composition. Emphasize has been placed on samples from Cerro del Fraile (CF) which represent, whether metasomatized by a hydrous fluid or a slab melt, fragments of a mantle wedge once modified by a subduction component, and later entrained by the alkaline lavas during the slab window formation below Patagonia. To our knowledge, no Li isotopes have ever been measured in xenoliths from the mantle wedge so far. All the samples are spinel-facies peridotites (dunite, lherzolite, harzburgite, and websterite) and were characterized into five groups, from CF1 to CF5.

Investigations have focused on *in-situ* measurements of Li (and B) concentrations and isotope ratios by SIMS of co-existing minerals, as well as trace element and REE concentrations (Sr, Y, Ce, Pr, Gd, Yb) in pyroxenes. Some mantle minerals seem to display systematic δ^7Li difference (e.g. 1.5% between clinopyroxene and olivine). We have intended to measure δ^7Li on the same pair of minerals (olivine-pyroxene) in our samples to see if such an isotopic fractionation is systematic in all mantle xenoliths, or if it varies between xenoliths coming from different geodynamic environments.

Measurements have been organised on three one-week sessions. The first session was performed in May 2008 and allowed measurements of samples from both Pali Aike and Cerro del Fraile. The second session (September 2008) concentrated on samples from Cerro del Fraile and on Li isotopes and concentrations. The third -and last- session has been scheduled for May 2009, in order to complete the dataset on CF and investigate samples from Marsabit.

Results

The samples from Pali Aike did not reveal any interesting intra- or inter- mineral zoning patterns and, therefore, were not investigated further. Results obtained on Boron display a random distribution of the concentrations (probably due to a resetting) through the clinopyroxenes investigated during the first session of analyses. Boron was not included in the analytical list later on.

Very interesting profiles were realised in samples from Cerro del Fraile. Preliminary results show a large variability within grains. Such isotopic variability has been previously attributed to diffusive fractionation of Li isotopes, within mineral phases and along melt pathways that pervade xenoliths [5]. Li concentration range from 1.0 to 1.8 ppm in olivines (with values up to 3.8 ppm found in dunite), and from 0.9 to 4.2 ppm in clinopyroxenes. The lowest concentrations were generally found at the rim. However, Li display opposite patterns in the dunite grains (CF3). Li isotope ratios range from -18.5‰ to 21.3‰ in olivines and between -26.1‰ and +8.1‰ in clinopyroxenes. The core is generally

represented by a plateau of light isotopic composition and the rim by a peak of higher δ^7Li values for most of the minerals, the CF3 olivines excluded. Concentrations in Sr follow those obtained for Li, whereas Y, Gd, Yb concentrations mimic the concentrations obtained for Ce. We are also currently investigating in details trace elements and REE contents of parallel profiles by LA-ICPMS.
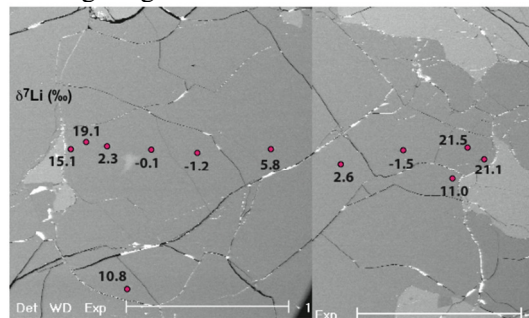
Fig. 1 BSE image of an olivine in sample Xe31(II) from the CF5 group. The measured profile is represented by the red dots, associated with the δ^7Li values. Corresponding patterns of Li isotopes and concentrations are represented below.
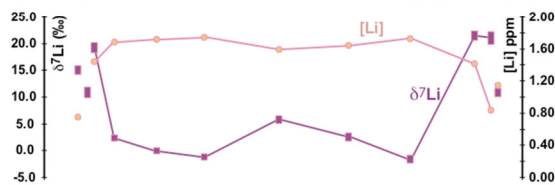
Fig. 2 Profile measured in a CPX from sample Xe22 (fine-grained spinel lherzolite ; Group CF1)
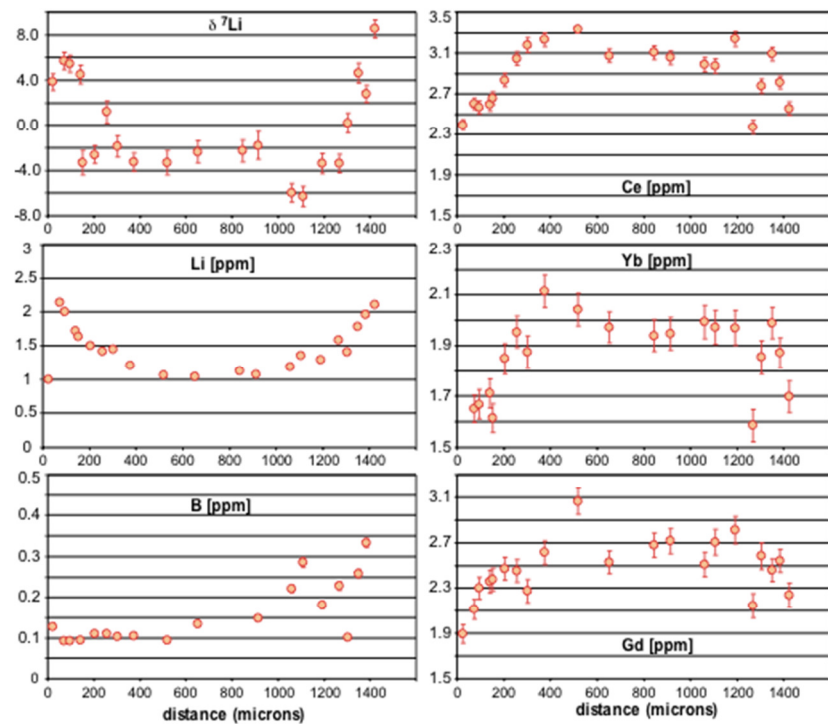
Data are currently being interpreted, and used for simulation of diffusion processes [6]. The upcoming last session of measurements will help us to establish a complete and comprehensive dataset for the different groups of samples from Cerro del Fraile, in order to explain the differences obtained between these groups and possibly obtained between the different localities (e.g. Marsabit). Once all the analyses completed, the dataset and interpretations will be compiled and written up for publication.

References
[1] R. Kilian & C.R. Stern, Eur. J. Min. 14 (2002) 25-36.
[2] C.R. Stern, R. Kilian, B. Olker, E.H. Hauri & T.K. Kyser, Lithos 48 (1999) 2217-2235.
[3] B. Kaeser, A. Kalt & T. Pettke, J. Petr. 47 (2006) 2149-2184
[4] B. Kaeser, A. Kalt & T. Ludwig, G-Cubed (2007)
[5] A.B. Jeffcoate, T. Elliott, S.A. Kasemann, D. Ionov, K. Cooper & R. Brooker, Geochim. Cosmochim. Acta 71 (2007) 202-218.
[6] L.A. Coogan, S.A. Kasemann, & S. Chakraborty, EPSL 240 (2005) 415–424.

High-resolution $\delta^{18}O$ analyses of two recent brachiopod shells

Proterozoic crustal evolution of the Northern Australian Craton from oxygen and hafnium isotope systematics of detrital zircons

A.I.S. Kemp[1]

[1]School of Earth and Environmental Sciences, James Cook University, Townsville QLD 4811 Australia

Aim

This project is to understand what caused the rapid growth of the Australian continent during the Proterozoic era, 1.9 to 1.5 billion years ago. This period corresponds to a global pulse of igneous activity during which almost half of the present Australian mainland formed, in addition to some world-class Cu-Au-U deposits (e.g. Olympic Dam, Mount Isa). The causes of this major magmatic upheaval remain enigmatic. In particular, the role of plate tectonic processes like those operating at the present, as opposed to plumes of hot material rising from deeper within the Earth, are intensely debated. I aim to address this problem through the oxygen and hafnium isotope analysis of the mineral zircon, which are a powerful tracer of crustal processes and uniquely preserve the record of ancient continental growth.

Methods

The first part of this project involved the in situ analysis of oxygen isotopes from detrital zircons of Proterozoic metasedimentary rocks from across northern Australia. These measurements were undertaken on sectioned zircon crystals in polished epoxy resin mounts, whose (U-Th)-Pb isotope crystallisation ages were previously determined by SHRIMP II at Curtin University of Technology, Perth. The oxygen isotope data were acquired at the University of Edinburgh with a Cameca ims 1270, using a 6 nA primary $^{133}Cs+$ beam and charge compensation by normal incidence electron gun. Secondary ions were extracted at 10 kV, and $^{18}O^-$ and $^{16}O^-$ were monitored simultaneously on dual Faraday cups. Each analysis involved a pre-sputtering time of 45 seconds, followed by data collection in two blocks of five cycles, amounting to a total count time of 40 seconds. Only zircons with concordant (U-Th)-Pb isotope systematics and an absence of cracks and inclusions were targeted.

A critical analytical issue to be overcome at the start of this study is that most of the sample mounts did not contain standard zircon chips that were suitable for the correction of instrumental mass fractionation (IMF) (with the exception of two mounts that included the Temora 2 standard). Instead, each mount contained chips of the multi-grain U-Pb age standard, zircon QGNG (1852 Ma), the O isotope characteristics of which were unknown. At the outset therefore, several chips of QGNG were embedded in an indium holder and added to the EIMF O isotope standard block for cross calibration of $^{18}O/^{16}O$ against accepted standards 91500 ($\delta^{18}O$ 10.07 ± 0.03‰ VSMOW) and KIM-5 ($\delta^{18}O$ 5.09 ± 0.03‰ VSMOW). The oxygen isotope composition of QGNG was also calibrated against Temora-2 ($\delta^{18}O$ 8.20 ± 0.03‰ VSMOW) in one sample zircon mount. Thereafter, QGNG was used as a monitor of IMF for the sample zircons using the previously determined average SIMS $\delta^{18}O$ value, pending more precise determination of $^{18}O/^{16}O$ by laser fluorination analysis (a 6 mg aliquot of QGNG was sent to J. Valley for this purpose). Specimen exchanges were also regularly conducted throughout each session to enable periodic analysis of 91500 and KIM-5 chips on the EIMF standard block. This reduced the number of sample zircon analyses possible each day, but was essential for monitoring instrument stability and to check for heterogeneity in QGNG between and within sample mounts.

Results

Besides 91500, a total of 1002 O isotope analyses were obtained during this study, of which 175 were from KIM-5, 367 from QGNG and the remainder from sample zircons. Analyses from zircon KIM-5 yielded an average $\delta^{18}O$ of 4.97 ± 0.46 ‰ (2 SD) [Figure 1], identical to the laser fluorination value (5.09‰ SMOW). The data from QGNG and the sample zircons are discussed separately below.

1. QGNG calibration and homogeneity

The initial experiment to calibrate QGNG against 91500 in the EIMF standard block yielded a mean $\delta^{18}O$ value of 7.22 ± 0.71 ‰ (2 SD, n = 20). Twenty analyses of KIM-5 run under the same conditions

returned $\delta^{18}O$ of 4.86 ± 0.48 ‰ (2 SD). Minor heterogeneity was therefore suspected in QGNG on the basis of these preliminary data. However, subsequent calibration of QGNG against Temora-2 in a sample mount yielded an identical, but significantly more precise $\delta^{18}O$ value of 7.30 ± 0.51 ‰ (2 SD, n = 35). Transmitted light and CL images were available for the QGNG chips in this mount, which thus allowed more careful targeting to avoid cracks and high-U (i.e. CL dark) areas of the grains; such features may have contributed to the lower reproducibility of O isotope analyses measured from QGNG in the EIMF standard block.

Figure 1 shows all analyses obtained from QGNG in the sample mounts during the course of this study, where the data are normalised to bracketing analyses of 91500 in the EIMF standard block (i.e. after periodic specimen exchanges). The reproducibility of these analyses (± 0.58 ‰ at 2 SD) is commensurate with that of KIM-5 (± 0.46 ‰), from which it can be concluded that QGNG is approximately homogeneous at the scale of sampling afforded by SIMS microanalysis, provided that high-U rims are avoided. The mean $\delta^{18}O$ value of all analyses (7.23‰) is indistinguishable from that determined by laser fluorination at the University of Wisconsin (7.18 ± 0.06 ‰, 2 SD, from 2 separate 2 mg splits, J. Valley pers. comm. Nov 2008). This confirms the suitability of QGNG for the normalisation of sample zircon $\delta^{18}O$, and demonstrates that, under favourable conditions of instrument stability, accurate O isotope data can be obtained using zircon standards located on a different mount.
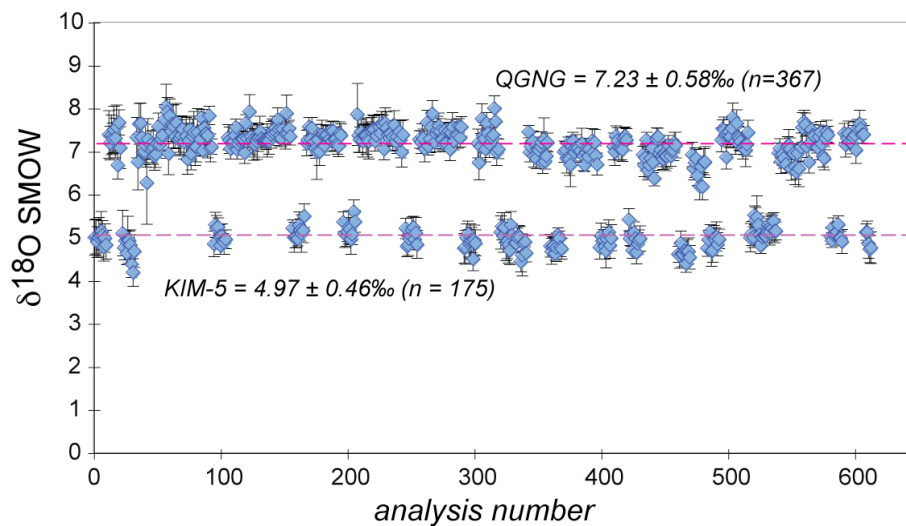
Fig. 1 SIMS O isotope analysis of zircons KIM-5 and QGNG corrected to bracketing analyses of 91500 (averages quoted at ± 2 SD). Dashed horizontal lines show the laser fluorination values for each zircon.

2. Sample zircons

Analyses were obtained from detrital zircons of 13 Paleoproterozoic greywackes from across northern Australia. These grains ranged in age from ~1650 to ~2900 Ma, although in detail the age spectra differs between samples. Collectively, the data show marked secular variation, whereby average $\delta^{18}O$ rises from uniformly mantle-like values of 5-6 ‰ at 2900-2650 Ma to a much larger spread of values by 1870 Ma (6-11‰), before again decreasing to lower values (6-8‰) in the youngest age populations (<1700 Ma). The full significance of these intriguing trends will not be clear until Hf isotope data are obtained from the same grains. However, the falling $\delta^{18}O$ after 1870 Ma is consistent with enhanced juvenile input and/or decreased recycling of sedimentary materials by the parental magmas to the zircons. In turn, this implies a greater proportion of new crust formation in the latter part of the Paleoproterozoic period in Australia, thus coinciding with the incipient break-up of the oldest hypothesised super-continent, Columbia.

Geochemical variation and characterisation of fine-grained volcanic ash

C.S.Lane[1] & S.P.E. Blockley[2]

[1] Research Laboratory for Archaeology, University of Oxford, Oxford, OX1 3QY, UK
[2] Department of Geography, Royal Holloway University of London, Egham, TW20 0EX, UK

Scientific rationale for study

One day of access to the IMF was sought in order to carry out a pilot study, as to the potential of using the ion microprobe for trace element characterisation of very fine grained vitreous volcanic ash. Tephrochronology has become an integral tool in the dating and testing of Quaternary palaeoclimate models, allowing correlations of palaeo-proxy archives over extreme distances. Whilst tephrochronological studies and the means of identification of large, visible volcanic ash units are well established, recent advances have led to the increasing use of very fine grained vitreous ash deposits (termed "microtephra"). Microtephra deposits can be deposited thousands of kilometres from the volcanic source [1], therefore atmospheric and aeolian sorting ensure that often only the vitreous fraction is remaining and single grain chemical analysis is necessary to identify the ash to the eruption event. Electron probe microanalysis is used to analyse oxide weight percent compositions of around 9 major elements and this is commonly enough to identify the eruption that produced the deposit. Cases are however regularly found where more than one micro-tephra deposit is of the same composition, usually from a single volcanic source, and they cannot be told apart using major elements alone.

Trace element analysis should aid the differentiation of apparently "indistinguishable" tephra deposits by showing more unique variability in response to differentiation processes acting on the melt. Previous studies on larger single grains of volcanic glass, using both Laser Ablation inductively couple Plasma mass spectrometry (LA-ICPMS) and Secondary Ion mass Spectrometry (SIMS) have proven this method is capable, at least in certain cases, of helping to discriminate and correlate volcanic ash deposits [2,3]. These methods however had not been tested on extremely fine grained material (sub 80 microns), and the ion microprobe was deemed to be the ideal instrument for analysing such samples, having a better spatial resolution than can be achieved on vitreous material by LA-ICPMS.

The samples analysed were a case study from Christine Lane's PhD, which aimed to test methods of characterisation and differentiation for chemically similar microtephra deposits. Two samples were chosen, from a suite of chemically similar (trachytic) Italian Late Quaternary tephra layers, both from the same lacustrine sedimentary record, well defined by their stratigraphy. This work was attempted with also on the laser ablation facility at Royal Holloway University of London, and the two methods compared and contrasted.

Results

In one day of analysis around 20 data points were gathered on individual vitreous grains from each of the samples. This allowed a good comparison to be made between the chemical compositions of the two ash deposits. As anticipated, some differentiation of the two ash layers was possible using this data, with the variability in composition of one ash being significantly greater than the variability of the other, which had a similar, but altogether more homogeneous composition. Whilst these compositional differences were very subtle, both tephra deposits showing alkali-trachytic compositions, the careful use of multivariate analysis techniques allowed the samples to be told apart (figure 1). The similarity of the samples confirms their origin from the same magma source and volcanic system. However, variations in the Ba and Sr compositions suggest that the composition of one of the ashes was influenced significantly by variation in the degree of alkali and plagioclase feldspar fractionation. A number of samples were repeatedly analysed in order to assess the repeatability of the method and this was shown to be very good. However, there were discrepancies in the data when compared to subsequently measured LA-ICPMS data on the same samples. This is deemed to be due to instrument specific variation in quantification and standardisation.

These positive results are very important to highlight the use of the ion microprobe as a potential method for trace element characterisation of microtephra samples. As yet, no published LA-ICPMS studies have managed to produce accurate trace element analysis on vitreous tephra below ~20

microns, whereas the ion microprobe has the potential to be able to characterise much smaller samples. This is essential for the extension of Quaternary tephrochronological correlations across continents, which will allow a better understanding of environmental systems and palaeoclimatic teleconnections.
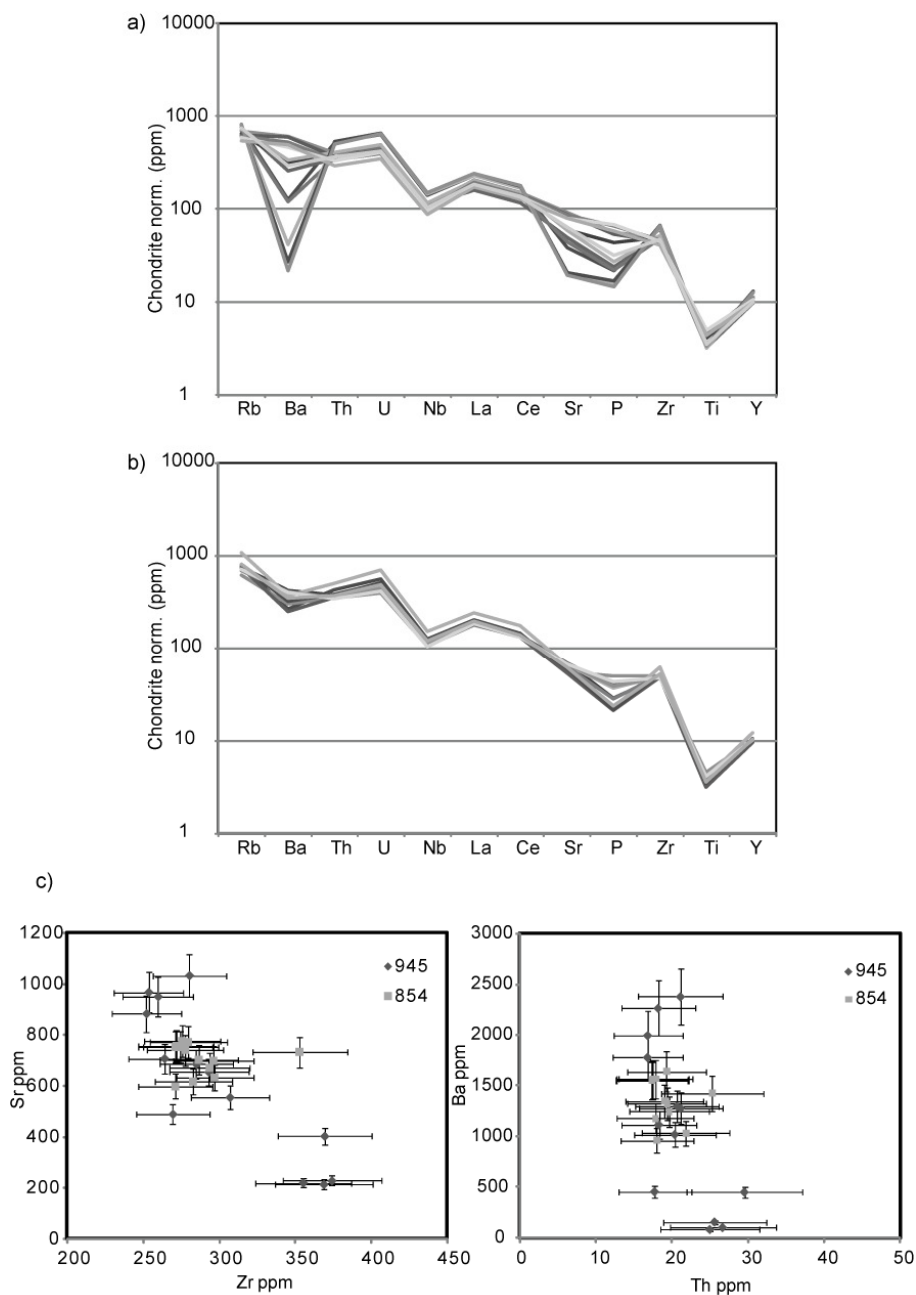
Fig. 1 Chondrite normalised trace element spider diagrams for the analysed samples a) sample OxT854 and b) sample OxT945. Each line represents an individual shard analysis. Note variability of OxT945, particularly in Ba and Sr. c) selected elemental bi-plots with two sigma uncertainty bars.

References
[1] S.P.E. Blockley, C.S. Lane, A.F. Lotter and A.M. Pollard, Quaternary Science Reviews 26 (2008) 3030-3036.
[2] N.J.G. Pearce, J.A.Westgate, W.T.Perkins and S.J. Preece, Applied Geochemistry 9, 13 (2004) 289-322.
[3] P. Clift and J. Blusztajn, Journal of Volcanology and Geothermal Research 92, 3-4 (1999) 321-347.

Trace element and volatile evolution in deep crustal hot zones:
An experimental case study of primitive basalts from St. Vincent

E. Melekhova & J. Blundy

Department of Earth Sciences, University of Bristol, Bristol BS8 1RJ, UK

Introduction

An understanding of the chemical evolution of a magma upon its ascent is fundamental to our knowledge of the processes of arc volcanism. The ultimate source of arc magmas lies within the peridotite mantle wedge. However, it is very unusual for a volcanic arc to erupt primitive (i.e. mantle-equilibrated) magmas, because most mantle-derived magmas undergo chemical differentiation prior to eruption.

We apply high-temperature, high-pressure equilibrium experiments to study the chemical evolution of arc magmas at Soufriere St. Vincent, Lesser Antilles. The aim of our experiments is to determine under what conditions (pressure, temperature and H_2O content) the derivative experimental melts match the erupted magmas of St Vincent and whether under those conditions our experimental phase assemblages match those of the cumulate xenoliths from the island.

Experimental run products were analysed for major elements by electron-microprobe at Bristol and for trace elements and volatiles (H_2O and CO_2) by ion-microprobe. Measurement of H_2O in melts enables us both to test that our experimental techniques do not result in H_2O loss, and also to accurately measure the H_2O content of melts at each condition, which is necessary for further constraints. Our approach will help constrain under which conditions mantle-derived magmas crystallise and differentiate beneath St Vincent.

This report presents work that forms part of a larger project, which involves, in addition to experimental petrology, numerical modelling and analogue experiments. The aim of the project is to test the model developed by Annen *et al* (2006) for the development of deep crustal hot zones beneath volcanic arcs via the emplacement of a succession of basaltic sills.

Results

During our first session on the ion-microprobe eight experimental run products were analysed. These experiments were performed on an MgO-rich, synthetic St. Vincent basalt at 1 GPa with H_2O contents of 2.3 wt% and 4.5 wt%, added as hydroxides.

Our first results lead us to very important conclusions for magma evolution. The proportions of melt and solids do not change linearly with temperature. The evolution of melt fraction with temperature (Figure 1) shows a sudden change from 60 to 30 % over just 30 °C (experiments with 2.3 wt % H_2O) and from 70 to 54 % within 50 °C (experiments with 4.5 wt% H_2O). This abrupt change in melt fraction, caused primarily by amphibole entering the crystallisation assemblage, will lead to the dramatic change in composition and rheology of the magma. The ion-microprobe measurements of H_2O show that our experimental technique does not result in significant loss or gain of H_2O due to H_2 diffusion through the capsule walls.

Our CO_2 measurements were not as successful as those for H_2O. For the CO_2 we are expecting similar behaviour as for H_2O, with decreasing temperature leading to the melt becoming CO_2-saturated. However, our ion-microprobe data are inconsistent. In experimental run products with initial 2.3wt% H_2O, CO_2 concentration increases with decreasing temperature, as expected. However, with 4.5 wt% of H_2O the opposite is observed. A further problem is that CO_2 concentration in all run products is much higher than we expected based on the CO_2-free nature of starting materials. More work has to be done during our next ion-microprobe session on CO_2 measurements, particularly the elimination of $^{24}Mg^{2+}$ interference on ^{12}C in Mg-rich basaltic melts.

It is too early to make any conclusions on our trace elements measurement, although we were able to measure all of the added trace elements in melt and crystal phases. Our preliminary data show that

trace elements are distributed homogeneously throughout the experimental melts and change consistently with temperature as expected for equilibrium conditions.
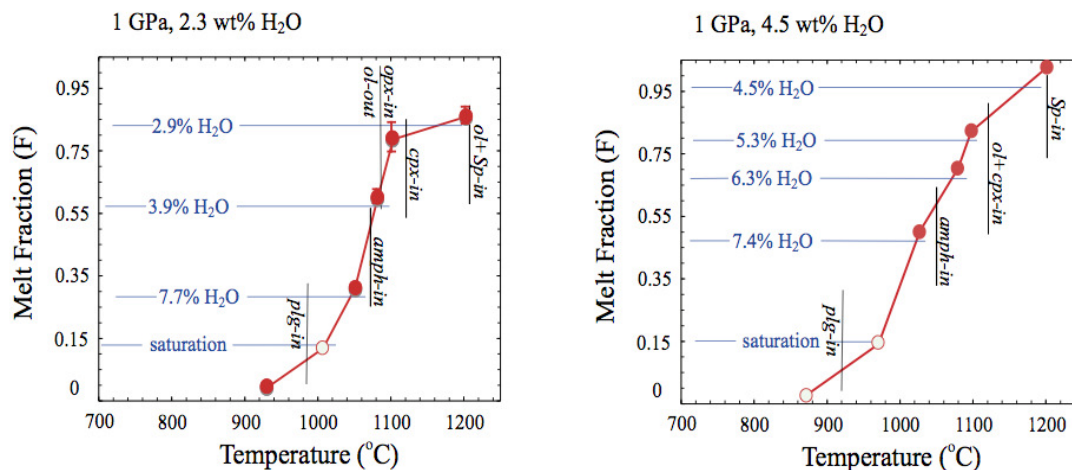
Fig. 1. Experimental results showing melt fraction (from mass balance) verses temperature. H_2O contents of melts based on ion-microprobe measurements are shown as horizontal lines. The variation of H_2O with crystallisation is consistent with closed system crystallisation without H_2O loss or gain from the experimental charges. Major phase boundaries are shown as vertical lines. Open circles are estimated temperature. Opx - orthopyroxene, cpx – clinopyroxene, ol – olivine, amph – amphibole, Sp –spinel.

Future Work

We have now generated experimental run products at 1.3 and 0.7 GPa with 2.3 and 4.5 wt% H_2O and these will be analysed during our next analytical session. Preliminary data on H_2O content of experimental olivines suggests that this may also be a fruitful avenue for further investigation.

Reference

[1] Annen et al. (2006), *J. Petrol.* **47**, 505-539

Li isotope determination of cooling rates

Philip Pogge von Strandmann and Tim Elliott

Department of Earth Sciences, Bristol University, Bristol, BS8 1RJ, UK

Overview

The aim of this study has been to investigate further Li isotope zonation discovered in natural crystals, which has been attributed to diffusive fractionation [1]. These observations point to an important application of Li isotope measurements in geospeedometry. However, the basic driving forces behind such diffusion are not well understood and so the implications of the zonations are ambiguous. The partition coefficients of Li between different minerals and melt should increase (variably) with decreasing temperature and it has been proposed that this mechanism may drive Li diffusion in a final stage of magmatic cooling [2]. We have tested this by looking at Li exchange between different minerals that have experienced different cooling histories, notably in rapidly and slowly cooled xenoliths. By examining a range of different minerals we obtain data on relative diffusivities to provide an empirical reference against a growing dataset of experimentally determined values. We made analyses during two 5 day sessions in June and December 2008, making Li isotopic and elemental profiles across coexisting clinopyroxene, orthopyroxene and olivine from several different peridotite xenoliths.

Equilibrated samples

Xenoliths from the Avacha mantle wedge have been in contact with metasomatic fluids [3]. From the whole-rock point of view, these xenoliths show a trend of increasing Li concentrations and heavier isotope ratios, suggesting interaction with an isotopically heavy fluid with high Li concentrations. This is consistent with hypothesised addition of fluids from the dehydrating subducting slab. This event is assumed to have occurred sufficiently long before eruption for the added Li to have diffusively equilibrated between phases. These xenoliths were found in a tuff deposit, meaning that post-eruption cooling has been rapid, with little time for late-stage diffusive fractionation.

Fig. 1 SEM image showing extent of fluid alteration of Avacha xenoliths. Below is shown SIMS data, demonstrating isotopic homogeneity.
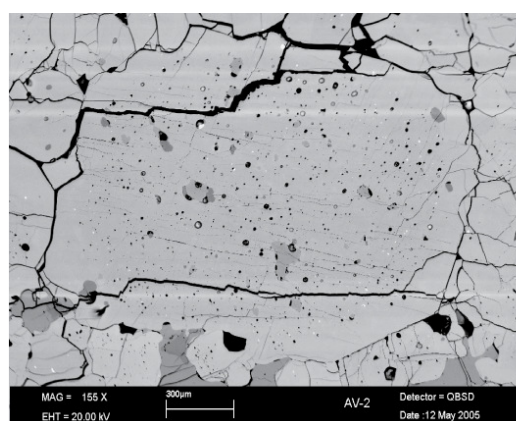
Sample Av2 shows evidence of extensive metasomatism, including trapped fluid inclusions (Fig. 1). However there are no significant isotopic differences in δ^7Li values between phases. Although there are Li concentration gradients across mineral boundaries, these are all within inferred equilibrium partitioning values, suggesting that these crystals were not perturbed subsequent to interaction with slab-derived fluids. This confirms the notion that much Li isotopic disequilibrium in xenoliths may be driven by diffusion during final cooling.
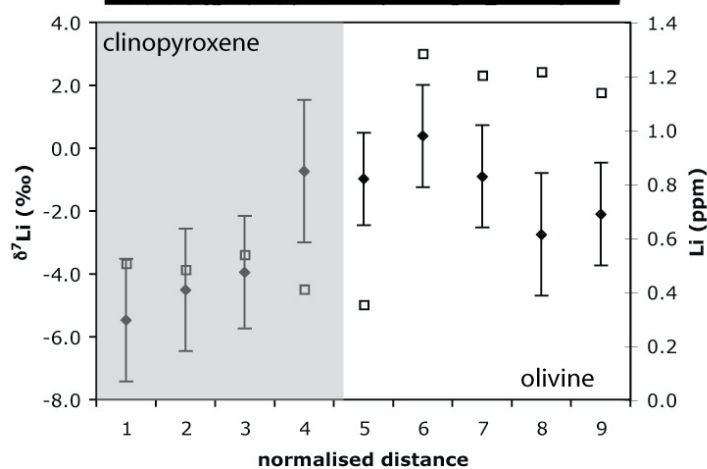
Fractionated samples

As a contrast to the isotopically equilibrated samples, we analysed minerals from a xenolith with an anomalously light whole-rock δ^7Li value. This xenolith is from Tok (Siberia), and has similarly experienced a high degree of metasomatism, but was notably erupted in a (slow-cooling) basalt flow.

Fig. 2 SIMS profile showing isotopic heterogeneity of Tok 6-3.
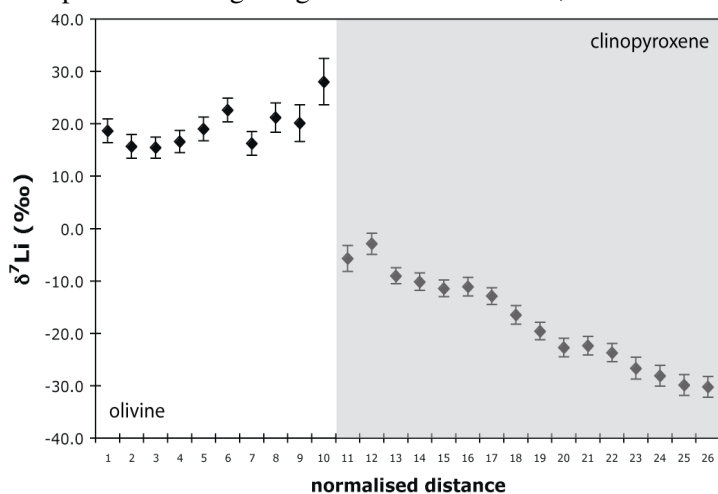
Mineral separate analyses by MC-ICP-MS indicate >20‰ difference between olivine and clinopyroxene, and this has been interpreted as evidence of late-stage diffusive alteration [4]. Therefore we measured profiles across co-existing olivines, orthopyroxenes and clinopyroxenes. These transects show extreme intra-mineral isotopic variation, but no classic isotope diffusion profiles (Fig. 2). This suggests that there are still aspects of diffusion, both mechanisms and driving forces, which we do not fully understand.

Matrix effects

Until now it has been difficult to directly compare MC-ICP-MS to SIMS Li isotope analyses because most crystals are heterogeneous. However analyses of the equilibrated Avacha xenoliths, which are isotopically fairly homogenous on the crystal scale, allow direct comparison between MC-ICP-MS and SIMS. For example, the olivines from sample Av4 measured by SIMS give a result of -1.9 ± 5.4‰ (2σ). Generally the 2σ uncertainty reported by the SIMS on these olivines (~1ppm Li) is ±2‰,

Fig. 3 Comparison of SIMS (closed symbols) to MC-ICP-MS (open symbols) isotope measurements.
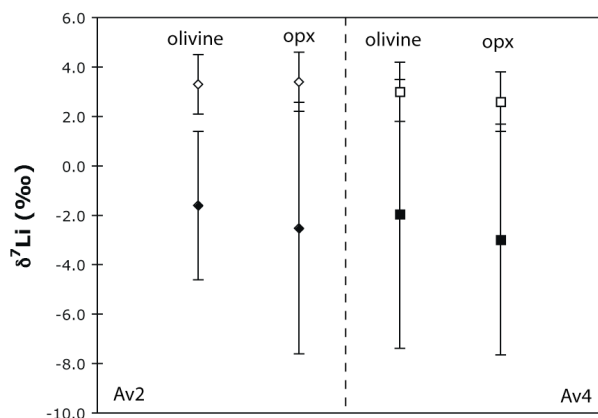
meaning that these isotopic variations cannot be resolved. In comparison, solution measurements of mineral separates (which is taken to be a "true" reference) give δ^7Li = +3.0 ± 1.2‰ [3]. For all measured Avacha olivines and orthopyroxenes, the $\Delta^7Li_{MCICPMS-SIMS}$ is 5-6‰, which means that while most of these measurements cannot be resolved from MC-ICP-MS measurements, there is a consistent offset towards lighter values of ~5‰ for the SIMS isotope analyses. (Fig. 3) In contrast, Li concentration measurements of solution compared to SIMS are identical.

Summary

- We have analysed unzoned, compositionally and isotopically equilibrated mantle xenoliths which were erupted in rapidly cooled tuff. This suggests that it is possible in some instances to analyse mantle Li isotopes which have not been altered by post-eruptional cooling.
- In contrast, xenoliths erupted in slow-cooling basalt show high degrees of isotopic variation, which is almost certainly due to diffusive fractionation during pre-or post-eruption cooling. These profiles will now be modelled to assess the role of Li isotopes as a geospeedometer.
- Measurements of unzoned samples allow assessment of matrix effects on SIMS measurements, compared to chemically purified solution MC-ICP-MS analyses. SIMS data are consistently offset towards lighter values by ~5‰.

[1] Parkinson, I.J., et al., Earth Planet. Sci. Lett. 257(2007) 609-621. [2] Jeffcoate, A.B., et al., Geochim. Cosmochim. Acta 71(2007) 202-218. [3] Ionov, D.A., et al., Earth Planet. Sci. Lett. 266(2008) 316-331. [4] Rudnick, R.L., et al., Earth Planet. Sci. Lett. 256(2007) 278-293.

The melt inclusion record of magma storage and degassing at Piton de la Fournaise, Reunion Island

D.M. Pyle[1], S.J.Collins[2]& J. Maclennan[2]

[1] Department of Earth Sciences, University of Oxford, Oxford, OX1 3PR, UK
[2] Department of Earth Sciences, University of Cambridge, Cambridge, CB2 3EQ, UK

Introduction

Reunion is a major basaltic shield complex, famously linked to the Deccan 'hotspot' trail. Piton de la Fournaise, the youngest volcanic centre on Reunion, has been particularly active since 1998, activity culminated in March/April 2007 with Reunion's largest eruption in 100 years.

We sampled olivine hosted melt inclusions from this eruption to determine the volatile and semi-volatile degassing record at the end of the most recent eruptive cycle at Piton de la Fournaise and to compare it to the beginning of the cycle (1998, Bureau et al., (1999)). Each melt inclusion was analysed for major elements and S by electron microprobe on a CAMECA SX100 at the University of Cambridge and for volatiles (H, CO_2, F, Cl) and trace elements (e.g. Li, Zr, La) by SIMS, on the Cameca IMS-4f ion microprobe at the University of Edinburgh.

Parallel work

Evidence suggests that semi-volatile trace metals are also degassed at volcanoes (Aiuppa et al., 2001). Therefore in parallel to the ion probe work a selection of melt inclusions were analysed for trace metals (Cu, Zn, Pb) by LA-ICP-MS at the University of Cambridge. These results are compared to the major volatiles analysed by SIMS to track degassing. The effect of S saturation on the behaviour of these elements was also investigated, by determining the sulphide-melt partition coefficients of these metals by analysing sulphide globules trapped within interstitial glass within Piton de la Fournaise cumulates by LA-ICP-MS (University of Quebec).

SIMS results

Water concentrations in the Reunion 2007 melt inclusions vary from 0.08 to 0.81wt%. These values are consistent with what has been suggested for Reunion melt inclusions previously (0.59-1.10wt%, Bureau et al., (1998)). Matrix glass has low degassed water contents (0.09-0.16wt%). The CO_2 concentrations are high, in 2002 they range from 390 to 2467ppm, and in 2007 they remain high but are relatively lower (271-1117ppm). Unlike the water contents in the matrix glass, the CO_2 concentrations (169-1105ppm) are of a similar range to the 2007 melt inclusions.

Discussion

When the CO_2-H_2O systematics of 2002 and 2007 are compared to the 1998 volatile compositions measured by Bureau et al., (1999), they show a continuation of a degassing trend, which began in 1998 at the beginning of the current eruptive cycle (1998-2007). The 1998 inclusions start with higher CO_2 and H_2O but show little evidence for low pressure degassing, due to rapid ascent from depth and therefore no melt entrapment. In contrast the 2002 and 2007 melt inclusions show evidence for shallower level degassing as the eruptive cycle continues. This may be representative of longer storage at a shallower depth over time. Vlastelic et al., (2007) interprets changes in the Pb isotope systematics and other compositional parameters to reflect increased contamination and magma recharge events. Vlastelic et al., (2007) proposes that sometime before 1998 new magma in-fills from depth, between 1998 and 2004 these magmas are stored and become progressively more contaminated as deeper portions of a vertically zoned dyke are erupted. In 2005 there is an injection of a fresh batch of magma and presumably between then and 2007 the remaining magma is emptied. Our data shows that picritic magmas from 2007 were stored at a more shallow depth than those magmas in 1998. In addition trace element ratios such as La/Sm (which at ~3 represents plume melts and at ~1 represents oceanic crust contamination) do not correlate with CO_2 and H_2O concentrations but are variable and therefore do not show specific contamination depending on depth trapped.

Enhanced CO_2 at low H_2O concentrations is not well understood but a number of models may be invoked. Gas fluxing of CO_2 rich gas from depth is likely in the plumbing system, this may dehydrate

the magmas in H_2O at variable depths. Re-circulation of degassed magmas to depths where they can dissolve CO_2 may also be possible. High CO_2 in matrix glass may be due to slower diffusion of CO_2 into gas bubbles than H_2O, on degassing during eruption at the surface.

Li is an incompatible trace element, yet it shows variation when plotted against other incompatible elements. This variation may be due to degassing and is consistent with the general positive correlation with H_2O. Li however is not depleted in matrix glass but shows increasing concentrations that correlate well with the incompatibles this variation is due to ground mass crystallisation on eruption and cooling.
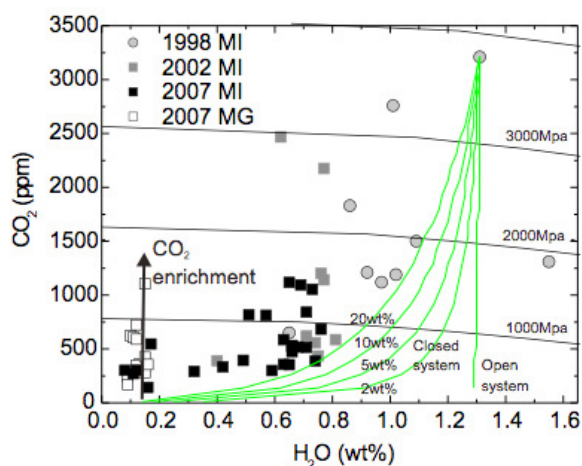
Fig. 1 Magmatic volatiles: Data from 2002 and 2007 melt inclusions and matrix glass compared to 1998 from Bureau et al., (1999). The data may be explained by closed system degassing > 20wt% exsolved vapour. At low water contents however some melt inclusions and matrix glass data appear enriched in CO_2. Isobars and degassing paths were calculated using Volatile Calc Ref. 5.
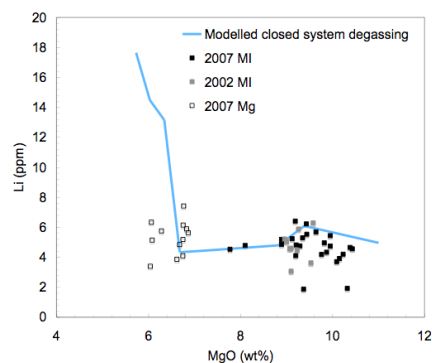
Fig. 2 Li systematics: Plot of Li against MgO in the melt inclusions and matrix glass. Closed system degassing was modelled to begin at 8.8wt% MgO. Li was modelled using $C_l = C_o F^{d-1}$. Degassing ceases and ground mass crystallisation then dominates in the matrix glass.

References

[1] Bureau, H., Metrich., N., Semet, M.P., Staudacher, T. (1999) *Geophysical Research Letters*, **26**.
[2] Aiuppa, A., Dongarra, G., Valenza, M. (2003) *Volcanism and the earth's atmosphere*, Geophysical monograph, **139**, (American geophysics union, Washington, DC, 2003)
[3] Vlastelic, I., Peltier, A., Staudacher, T. Short-term (1998–20.06) (2007) *Chemical Geology*, **244**.
[4] Newman, S., and Lowenstern, J.B. (2002) *Computers and geosciences*, **28**.

Cyanobacterial weathering of minerals

K. Vala Ragnarsdottir and Dana Kapitulčinová

Department of Earth Sciences, University of Bristol, Bristol, BS8 1RJ, UK

Introduction

Biological weathering plays one of the key roles in mobilisation of essential nutrients that are fixed in the lithosphere and thus provides the biosphere with necessary elements for its existence. Many organisms, such as some groups of bacteria, lichens, fungi and higher plants, have been shown to enhance the release of elements from minerals [1], [2], [3]. Cyanobacteria (photosynthetic oxygen-evolving bacteria) have hitherto not been thoroughly studied with respect to weathering under controlled laboratory conditions and thus their interactions with minerals are poorly understood.

In this study, we are interested in the surface structure and chemistry of minerals undergoing alteration induced by cyanobacteria. The current work is focused on colonisation and weathering of biotite by filamentous cyanobacteria under controlled laboratory conditions. We aim to reveal whether cyanobacteria cause any structural and/or chemical alteration to biotite surfaces. Magnesium, potassium and iron depletion at such mineral surfaces are of primary concern because these are essential nutrients for cyanobacteria.

The use of the ion probe in biological weathering studies is a novel approach. We are concerned about removal of the cyanobacteria from the mineral surface (required for some analytical methods) because it could also remove the mineral surface layers where weathering may have occurred and make it not possible to detect the changes. Therefore, we focused on depth profiling using the ion probe as this enables us to keep the bacteria in place on the mineral surface while analysing the chemistry of the mineral underneath the cells.

Methods

A number of depth profiles were undertaken through cyanobacterial filaments (~10 µm width) grown on biotite flakes (Figure 1) to reach and analyse the cell-mineral interface. We aimed to analyse as small biotite areas as possible underneath the filaments so that potential alterations on the cell-mineral interface, e.g. depletion in magnesium, potassium and/or iron, could be detected.
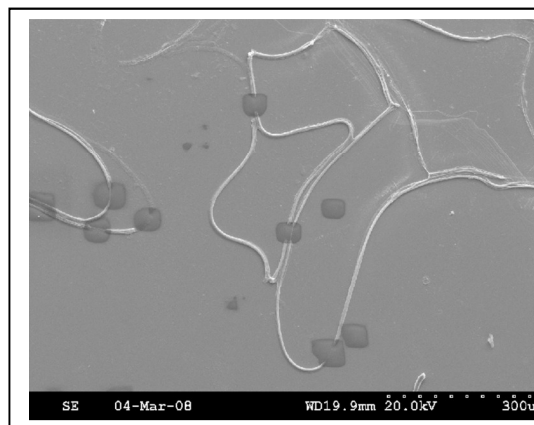
Fig. 1 Several etch pits after ion probe depth profiling through cyanobacterial filaments grown on the surface of a biotite flake.

Various operating conditions were applied in order to reveal that most suitable for analysis of the samples. Raster mode was selected over static mode and areas of 10 x 10 μm were rastered. In order to get the ion counts only from the 2-4 μm central part of the rastered area, i.e. where the filament was located, recording of secondary ions was restricted by gating. A primary beam current of 0.13 nA was used for most depth profiles. During a few depth profiles, we attempted to drill through the cell quickly using 0.5 nA or 0.145 nA before analysing the interface very slowly using a beam current of 0.035 nA (primary aperture employed). The isotopes ^{1}H, ^{12}C, ^{16}O, ^{19}F, ^{23}Na, $^{25/2}$Mg (to correct for C), ^{26}Mg, ^{27}Al, ^{30}Si, ^{31}P, ^{40}Ca, ^{41}K and ^{56}Fe were analysed for.

Results and Discussion

We were able to acquire some data from depth profiling of the cell-mineral interface. However, it was very difficult to interpret these data due to a number of issues.

Analysis revealed that the concentration of potassium in the filaments was roughly the same as that in the biotite - ^{41}K was stable throughout all profiles. As a result, even if there was some slight depletion of this element in the mineral it would be impossible to detect. The ion counts of magnesium and iron were a little lower on the interface relative to silicon suggesting depletion of these two elements on the biotite surface. Nevertheless, this "depletion" might have also resulted from slower stabilisation of the Mg and Fe ions relative to silicon and could have therefore been an artefact.

Another problem with the analyses was that we obtained aluminium signals even at the start of all profiles although there ought to have been no aluminium present in the cyanobacterial filaments. It is likely that the beam was rastering also some part of the biotite around the filament due to imperfections in the beam shape. Although we used the gate, there was obviously a contribution to the signal coming from the biotite around the filament that distorted the real information from underneath the filament.

The topography of the samples appears to be a major issue. Uneven sputtering of the material (bacterium and biotite) very likely gave us a mixed signal at the cell-mineral interface. We also did not know how much mixing of material there was due to the sputtering, i.e. the depth resolution.

Due to all of these factors, it was not possible to distinguish the real information from instrumental artefacts.

Summary

The results from the performed ion probe work have shown that the required sample analyses are very challenging even for the state-of-the-art instruments. Due to a number of reasons, it was not possible to obtain conclusive data supporting or denying the possible alteration of the mineral by the overlaying cyanobacteria. Alternative methods, such as transmission electron microscopy on cross sections through the cell-mineral interface, will be applied to samples in the future.

Nevertheless, it is important to highlight that the performed analyses were valuable in some respects. They revealed some very useful information about the capabilities and limitations of the Cameca ims 4f instrument and this knowledge can be used by other ion probe users interested in analyses of similar samples.

References

[1] Hutchens E, Valsami-Jones E, McEldowney S, Gaze W, McLean J. 2003. Mineralogical Magazine 67:1157-1170.
[2] Gadd GM. 2007. Mycological Research 111:3-49.
[3] Kelly EF, Chadwick OA, Hilinski TE. 1998. Biogeochemistry 42:21-53.

Ocean acidification during the Palaeogene hydrothermals

A. Ridgwell[1] & D. Schmidt[2]

[1] School of Geographical Sciences, University of Bristol UK
[2] Department of Earth Sciences, University of Bristol UK

Introduction

The environmental impact of increased atmospheric CO_2 (pCO_2) represents one of the great challenges for marine life in the near future [1]. In addition to an increase in surface ocean temperatures and stratification of the water column, an increase in seawater acidity via the incorporation of anthropogenic CO_2 into the surface ocean [2] will occur – a phenomenon known as 'ocean acidification'. Computer models have predicted a lowering of surface ocean pH by up to 0.5-0.6 pH units over the next 250 years, a transient change that is likely unprecedented in the last 300 Myr [2] and one with potentially very significant but currently highly uncertain consequences for calcifying organisms in the ocean and thus marine ecosystems. Reading the geological record of past ocean acidification events can provide critical help in reducing the uncertainty about future impacts.

The Palaeocene-Eocene thermal maximum ('PETM') was characterized by a 5-8°C temperature change [3] and is considered a Palaeo-analogue for future climate change. The event has been interpreted as driven or amplified by the catastrophic release of carbon to the ocean and/or atmosphere, perhaps as the result of the dissociation of a large amount of methane hydrates, with the inferred addition of CO_2 comparable to predictions of fossil fuel combustion over the coming centuries [4]. Although a significant decrease in seawater acidity is indicated by the observed dramatic dissolution of carbonates in deep-sea sediments we do not know the magnitude or rate of the pH change. Without this critical information we cannot extrapolate available observations biotic changes across the PETM to the future.

Boron isotopes are the only established proxy for reconstructing seawater pH [5]. However, traditional wet chemical methods for boron isotopes need 100 specimens >355 µm which are not available from any drilled PETM section to date. Recent improvements in the accuracy and precision of *in situ* measurements on marine carbonates using state of the art secondary ionisation mass spectrometry (SIMS) techniques at Edinburgh University enables us now to analyse element concentrations and B isotopes on selected chambers of individual foraminifers and hence reconstruct the pH of this palaeo-ocean acidification event.

Results

In previous measurement time using the Cameca ims-4f (see: 2007 IMF302/0507 project report), we measured boron isotope composition of deep sea dwelling (benthic) foraminifer *Oridorsalis umbonatus* at three modern sites (Site 1264, Site 1262 and Site 690B) with different pH and hence degrees of carbonate supersaturation and preservation in order to quantify the 'vital effect' (i.e. the breathing of the organism decreases the pH compared to ambient bottom water conditions). Partial dissolution of the foraminifer shells led to internal holes, dissolution of septa, and ultrastructural breakdown due to the decrease in carbonate saturation across the sites with carbonate undersaturation and strongest dissolution at site 690B. By using established δ^{11}B-pH relationships, based on the B isotopic measurements we calculated a slight declining seawater pH gradient going from Site 1264, through 1262, to 690B, which closely agrees with calculations made at these locations from observed ocean geochemical datasets. Furthermore, we found no systematic internal variability in benthic foraminifers, meaning that partial dissolution does not limit our ability to generate benthic pH records.

On the basis of this information, we analysed the B isotope of this species from Maude Rise, and documented a negative B isotope excursion and hence drop in ocean pH across the PETM event. Work is currently on-going in conjunction with Dr. Richard Hinton (NERC IMF) to

develop a robust protocol for calculating the analytical uncertainties in light of the technical challenges of measuring $\delta^{11}B$ values in small samples with relatively low boron content.

Further $\delta^{11}B$ measurements were made on samples from Bass River to confirm the global nature of the *p*H excursion. We also attempted to get a cross calibration between *Oridorsalis umbonatus* and *Lenticulina* sp. running. However, the specimens of *Lenticulina* were all too dissolved to yield sufficiently good data. This is related to the different wall structure and higher Mg making the species more dissolution susceptible.

The main focus of the last part of IMF302/0507 was to improve the trace element (TE) record for Maud Rise and Bass River Sites. Due to the previously established spatial homogeneity of the TE data and the need to improve the temporal resolution of the TE data, we concentrated on a small number of analyses in a large number of samples. We found that the reconstructed benthic temperature based on Mg/Ca during the PETM at both Sites was comparable to published estimates. Hence, we conclude that TE analysis allows the stratigraphic position of single foram samples to be confirmed in the same samples as B isotopic measurements, even in the absence of contemporaneous $\delta^{13}C$ measurements (which are the commonly used means of identifying position relative to the PETM excursion, but a measurement that is not possible on the ims-4f instrument).

References

[1] J.A. Raven, et al., Ocean acidification due to increasing atmospheric carbon dioxide, Policy document 12/5, Royal Society of London, London, United Kingdom, London (2005).

[2] K. Caldeira, M.E. Wickett, Anthropogenic carbon and ocean pH, Nature 425, 365 (2003).

[3] J.C. Zachos, U. Rohl, S.A. Schellenberg, A. Sluijs, D.A. Hodell, D.C. Kelly, E. Thomas, M. Nicolo, I. Raffi, L.J. Lourens, H. McCarren, D. Kroon, Rapid Acidification of the Ocean During the Paleocene-Eocene Thermal Maximum, Science 308, 1611-1615 (2005).

[4] G.R. Dickens, J.R. O'Neil, D.K. Rea, R.M. Owen, Dissociation of oceanic methane hydrate as a cause of the carbon isotope excursion at the end of the Paleocene, Paleoceanography 10, 965-971 (1995).

[5] N.G. Hemming, G.N. Hanson, Boron isotopic composition and concentration in modern marine carbonates, Geochimica Cosmochimica Acta 56, 537-543 (1992).

The evolution of the caldera-forming Rotoiti magma, New Zealand, revealed by plagioclase zoning and melt inclusions

V.C. Smith[1*], P. Shane[2] & I.A. Nairn[3]

[1] Department of Earth Sciences, University of Bristol, Wills Memorial Building, Queen's Road, Bristol BS8 1RJ

[2] School of Geography, Geology & Environmental Science, University of Auckland, Private Bag 92019, Auckland, New Zealand

[3] 45 Summit Road, Rotorua RD5 & GNS Science, Wairakei Research Centre, Taupo, New Zealand

[*] current address: Research Laboratory for Archaeology and the History of Art, University of Oxford, Dyson Perrins building, South Parks Road, Oxford OX1 3QY

Introduction

The aim of this study is to gain further insight into assembly of large volumes of silicic magma in the crust beneath the Taupo Volcanic Zone, New Zealand. Here we use the record preserved in the crystals from the most recent caldera-forming eruption (Rotoiti; 120 km^3 magma) and the subsequent Earthquake Flat eruption (EQF; 10 km^3) at ~55 ka. Plagioclase compositional profiles and melt inclusions (MI) were analysed using SIMS techniques, these data are coupled with electron microprobe (EMP) data to provide information on the processes that occurred within the magmatic systems prior to the eruptions, and further our understanding on the assembly of silicic magmas within the upper crust.

Summary of results

Plagioclase crystallises over a wide range of magmatic compositions and conditions, continuously recording variations in composition during crystallisation. Thus, profiles provide a fairly complete record of magmatic processes. Rotoiti and EQF plagioclase crystals show variations in both major (An_{36}-An_{68}) and trace elements (0-159 ppm MgO, 46-112 ppm TiO_2, 618-756 ppm Sr & 618-756 ppm Ba; Fig. 1). X_{An} is very sensitive to a range of parameters, e.g., temperature, pressure, H_2O, and melt composition, which change considerably during typical closed system processes like magma ascent. More insight into magmatic processes can be gained from the record of melt evolution that can be reconstructed from trace element compositions [1], using partition coefficients [2]. Calculated melt compositions display a wide range in MgO_{melt} (0-2 wt%), and extend to higher ranges than the matrix glass compositions (±0.12 wt%) indicating there was significant fluctuations in melt composition during the magmas residence in the upper crust. The high MgO_{melt} contents are recorded in specific zones that follow resorption horizons, and typically correspond to increases in X_{An}, MgO_{melt} and Sr/Ba. These notable increases in composition at resorption horizons are observed in other studies[1] and are direct evidence for recharge of the system by significantly more mafic melt.

Most of quartz-hosted MI are slightly enriched in Sr and MgO, and depleted in Ba and Rb relative to the matrix glass compositions. These variations between the MI and matrix glass are consistent with the crystallisation of predominately plagioclase assemblage following MI entrapment in their respective melts. However, some of the MI are more evolved that matrix glass (lower Sr and Ba concentrations) and imply that there was a recharge event after the entrapment of some of the melt inclusions. Enclosed MI from Rotoiti deposits have 3.41-6.65 wt% H_2O and 234-798 ppm CO_2. Other volatile elements display a similar diversity between the magmas, and are similar in both MI and matrix glass, with ranges of 26-64 ppm Li, 12-29 ppm B, 30-318 ppm F, and 263-500 ppm Cl. Entrapment pressures calculated using H_2O and CO_2 contents indicate crystallisation occurred between 100 and 260 MPa, and indicate the magmatic system was located ~4-10 km beneath the surface.

The large volume Rotoiti and smaller EQF systems both appear to have had a complex history, with periodic recharge events commonly entering these upper crustal silicic systems.

These recharge events appear to be a mechanism of adding more melt to the system and allowing them to accumulate to such large volumes.

Future work

All analyses have been completed and these data along with other electron microprobe data are currently being interpreted and written up for publication.

References

[1] V.C.Smith, J.D. Blundy & J.L. Arce. J Petrol 50 (2009) 405-426.

[2] I.N. Bindeman, A.M. Davis & M.J. Drake Geochim Cosmochim 62 (1998) 1175-1193.
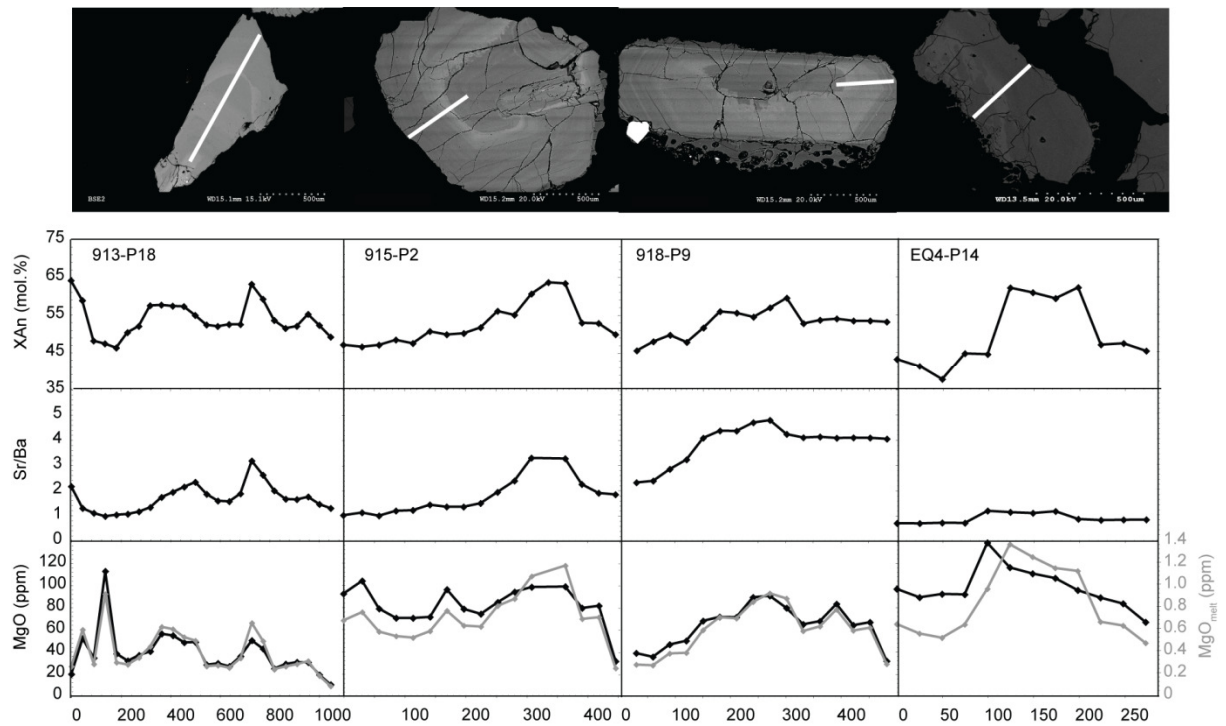
Fig. 1 BSE images, and major and trace element profiles across plagioclase crystals in the Rotoiti and EQF eruption deposits. Bottom axis is the distance (in μm) from the crystal rim. Noticeable major resorption horizons are observed on BSE images. Melt compositions (MgO$_{melt}$) determined from plagioclase compositions using partition relationships [2] indicate the zones that follow the resorption event crystallised in a less evolved melt.

Melt inclusion compositions of high ^{3}He/^{4}He picrites from Baffin Island and West Greenland

N.A. Starkey[1] & R.M. Ellam[2]

[1]School of GeoSciences, University of Edinburgh, Edinburgh EH9 3JW, UK
[2]Scottish Universities Environmental Research Centre, Rankine Avenue, East Kilbride, G75 0QF, UK

Justification

Lava flows were erupted 62 Ma in Baffin Island and West Greenland (BI-WG) at the start of volcanism in the North Atlantic Igneous Province (NAIP). Magmatism in the NAIP was voluminous with a rapid onset, producing lavas with high magnesium contents and associated high olivine crystal contents. Controversy has focused on the origin of the olivine crystals, particularly those with high forsterite (up to Fo$_{93}$) and whether they represent phenocrysts or xenocrysts. Another important feature of the BI-WG lavas is their extremely high ^{3}He/^{4}He, up to 50 R_a [1,2]. These lavas have the highest magmatic terrestrial ^{3}He/^{4}He suggesting that they sample the most primitive, undegassed reservoir available in the Earth. There has been much debate as to the trace element and radiogenic isotopic composition of the high-^{3}He/^{4}He reservoir. Recent studies have shown an apparent link between high ^{3}He/^{4}He and depleted mantle compositions [1,3,4]. However, Starkey et al. (2009) showed that extremely high ^{3}He/^{4}He occur in depleted and relatively enriched BI-WG lavas. Crustal contamination of originally depleted melts to produce the high-^{3}He/^{4}He relatively enriched melts has been ruled out in the whole-rocks [2]. The range in trace element and radiogenic isotope compositions displayed by the BI-WG lavas is not dissimilar to basalts commonly erupted at mid-ocean ridges [2]. However, derivation of the lavas from the convecting upper mantle source commonly assumed for mid-ocean ridge basalts (MORB) cannot account for the higher ^{3}He/^{4}He displayed by the early NAIP lavas or the inferred high temperature source [5,6].

Many studies have focussed on the whole-rock composition of the early NAIP lavas, with very few studies focusing on the melt inclusion compositions, particularly for high ^{3}He/^{4}He lavas. Compositions of melts trapped within olivine crystal inclusions have the potential to record the effects of crustal contamination and/or the presence of 'xenocryst' olivines. It was shown that melt inclusions in BI lavas may register up to an order of magnitude more crustal contamination than their associated whole-rocks [7]. However, it is unclear if high forsterite 'xenocrystic' olivine crystals also showed 'xenocrystic' melt inclusion compositions. This incompatible trace element melt inclusion study of high-^{3}He/^{4}He lavas allows for better assessment of the individual melt compositions that contribute to the lavas and helps to characterise the compositions that are associated with high ^{3}He/^{4}He. In addition, this study focuses only on melt inclusions in high ^{3}He/^{4}He lavas from BI-WG that cover a range of depleted to relatively enriched compositions (whole-rock ^{143}Nd/^{144}Nd from 0.512876 to 0.513053). If crustal contamination of the melt inclusions and the presence of an olivine xenocryst population in the transporting magma can be ruled out then the range in melt inclusion compositions represents that of the mantle source region.

Results

Trace element and REE compositions were measured in 72 olivine hosted melt inclusions in two BI and two WG high-^{3}He/^{4}He picrites. The melt inclusions analysed were generally small (~25μm in diameter) and were hosted in olivine crystals covering a range of forsterite contents. Only clean, glassy melt inclusions were chosen for analysis so that experimental reheating to homogenise the glasses was avoided. Prior to SIMS analysis, the samples were characterised for whole-rock major and trace element and radiogenic isotope ratios [2] as well as major elements on the melt inclusions and olivine hosts. These new melt inclusion data add to the data obtained in the one-day feasibility study undertaken on the ion microprobe in May 2007 on one of the samples used in this study (PAD6).

Melt inclusions within any one sample cover a wide range of compositions but the average composition reflects that of the associated whole-rock. Chondrite-normalised multi-element plots show that melt inclusions have higher concentrations of REE than their associated whole-rock (Figure 1). This feature is probably related to the high olivine content of the whole-rock (in many cases up to 40% crystals) which effectively acts to dilute the incompatible element concentrations. Importantly, REE profiles of melt inclusions are broadly parallel compared to their associated whole-rock. Crustally contaminated melts would be expected to show cross cutting profiles through LREE enrichment and this is not observed in the melt inclusions of this study. The WG melt inclusions are more LREE depleted than the BI melt inclusions, in agreement with the whole-rocks, but in general all profiles are fairly flat indicating the generally depleted nature of the source (Figure 1).

Early NAIP lavas can be compared to depleted 'normal' MORB (NMORB) and relatively enriched 'Icelandic' lavas on a plot of log(Nb/Y) against log(Zr/Y) (Figure 2). $\Delta Nb = 1.74 + \log(Nb/Y) - 1.92 \log(Zr/Y)$, with NMORB characterised by $\Delta Nb<0$ and Icelandic (or 'enriched' EMORB) lavas characterised by $\Delta Nb>0$ [8]. Figure 2 shows that samples with whole-rock negative ΔNb only contain melt inclusions with negative ΔNb (362077 and 400452) and samples with whole-rock positive ΔNb only contain melt inclusions with positive ΔNb (PAD6 and DUR8). This is an important observation as it rules out the possibility that high $^3He/^4He$ is present only in depleted melt compositions.
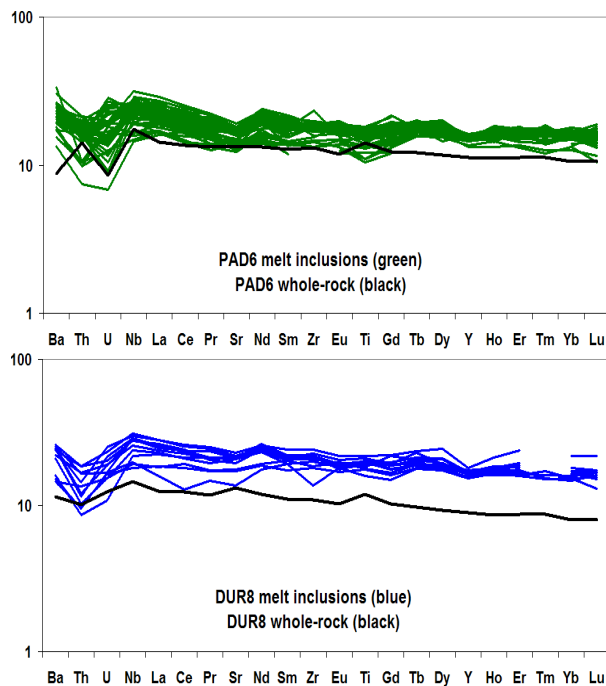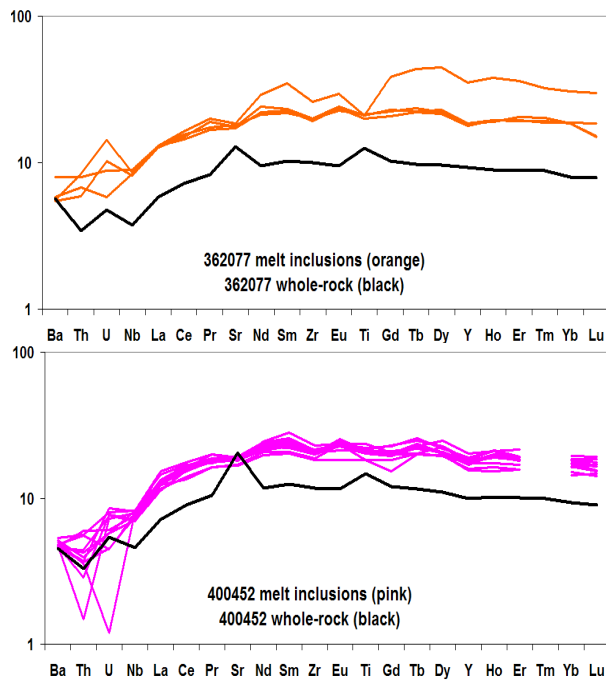
Fig. 1 Chondrite-normalised multi element plots for Baffin Island (PAD6, DUR8) and West Greenland (362077, 400452) melt inclusions and associated whole-rocks.
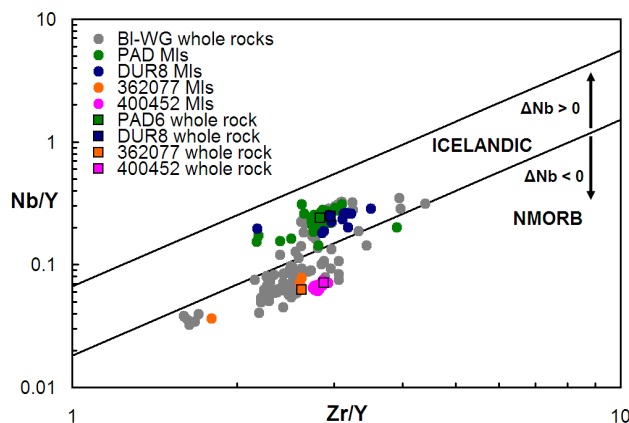
Fig. 2 log(Nb/Y) plotted against log(Zr/Y) for Baffin Island and West Greenland melt inclusions compared to their whole-rock compositions. Samples with positive ΔNb only contain melt inclusions with positive ΔNb.

Summary

This work supports the findings from the associated whole-rock study to conclude that high ^{3}He/^{4}He is a feature of both depleted and relatively enriched melt compositions. Samples that display relative enrichment in their whole-rocks contain only relatively enriched melt inclusions. This suggests that models requiring depleted residues of melting for the source of high ^{3}He/^{4}He cannot account for these data. The melt inclusions in the picrites of this study also support the earlier conclusion [2] that crustal contamination has not affected these high ^{3}He/^{4}He samples, although more modelling is yet to be carried out. The presence of xenocryst olivine populations is also ruled out such that the range in trace element compositions and lithophile radiogenic isotope ratios of the high-^{3}He/^{4}He picrites represents that of their mantle source. The mantle source for BI-WG lavas may be the depleted upper mantle except that helium with high ^{3}He/^{4}He has been added, possibly by diffusion, which can explain the decoupling of ^{3}He/^{4}He from incompatible trace elements and radiogenic isotope ratios.

References

[1] Stuart, F.M., Lass-Evans, S., Fitton, J.G., Ellam, R.M. Nature, 424 (2003) 57-59.
[2] Starkey, N.A. Stuart, F.M., Ellam, R.E., Fitton, J.G., Basu, S., Larsen, L.M. Earth Planet. Sci. Lett. 277 (2009) 91-100.
[3] Ellam, R.M., Stuart, F.M. Earth Planet. Sci. Lett. 228 (2004) 511-523.
[4] Class, C., Goldstein, S.L. Nature 436 (2005) 1107-1112.
[5] Larsen, L.M., Pedersen, A.K. J. Petrol. 41 (2000) 1071-1098.

[6] Herzberg, C., Asimow, P.D., Ardnt, N., Niu, Y., Lesher, C.M., Fitton, J.G., Cheadle, M.J., Saunders, A.D. Geochem. Geophs. Geosyst. 8 (2007) doi:10.1029/2006GC001390.

[7] Yaxley, G.M., Kamenetsky, V.S., Ka,enetsky, M., Norman, M.D., Francis, D. Contrib. Mineral. Petrol. 148 (2004) 426-442.

[8] Fitton, J.G., Saunders, A.D., Norry, M.J., Hardarson, B.S., Taylor, R.N. Earth Planet. Sci. Lett. 153 (1997) 197-208.

Probing the birth and growth of continents via isotopic records in titanite

C.D. Storey[1] and C.J. Hawkesworth[1]

[1] Department of Earth Science, University of Bristol, Wills Memorial Building, Queen's Road, Bristol, BS8 1RJ, UK

Introduction

Titanite is a promising candidate as a repository of chemical information relating to the growth of continental crust from the depleted mantle reservoir. It is LREE-MREE enriched and thus often contains elevated Nd (1-3000ppm), with an Sm/Nd of 0.1-0.2 typically. Such concentrations make titanite a candidate for in-situ measurement of Nd isotopes, which can be related to the development of the depleted mantle reservoir. In order to fully utilise this system, the titanite requires precise dating in order to calculate initial ratios, particularly due to radiogenic ingrowth of Nd within the host since crystallisation. This is best achieved through the U-Pb system. Also, oxygen isotopes help to constrain whether the host magma was from a juvenile melt from the depleted mantle or has been contaminated from sediments. In this way we can assess more fully the true growth of continental crust versus recycling of pre-existing crust. Much the same approach has recently become favourable in the mineral zircon [1,2] via the combined in-situ measurement of U-Pb, O and Hf isotopes. In this study, samples from the c.3.65-3.85 Ga gneisses (tonalities and granodiorites) surrounding the Isua Greenstone Belt of West Greenland have been studied by using the Cameca 1270 multicollector ion microprobe. Titanites have been analysed first for O isotopes and then subsequently for U-Pb isotopes. Zircons from certain samples have been measured for O. The ages have also been augmented by external work by ID-TIMS at NIGL and by LA-ICPMS at the Natural History Museum, London.

Results

Three samples for which U-Pb ID-TIMS age data [3,4] on titanite were available have been analysed as well as one sample for which zircon U-Pb SIMS data were available [5] and three more for which no previous age data were available. Figure 1 displays SIMS, LA-ICPMS and ID-TIMS data from titanites and zircons all samples analysed. It is apparent that there is a good agreement between all three methods for titanite, all corrected for common Pb by measurement of ^{204}Pb. Several samples from which zircons were also available for analysis or were previously analysed (JC130-99, JC133-99, JC200-00, SM/GR/98/2 and SM/GR/00/2) demonstrate that zircon ages are always older than titanite ages, but in two cases (JC130-99 and JC133-99) the titanite ages are close to concordia and the zircon ages and in another case (JC200-00) the titanites are discordant but discordia gives an upper intercept age close to the zircon age. It is also apparent that the ID-TIMS (from two different labs) are also in close agreement with the concordant or upper intercept ages for the titanites. In the case of SM/GR/98/2 the titanite ages are much younger (c.2.6 Ga) and cluster close to concordia; however, a few analyses by both ID-TIMS and LA-ICPMS are discordant with older ^{207}Pb/^{206}Pb ages and trend on a poorly defined discordia towards an upper intercept close to the zircon age. In sample SM/GR/00/2 all of the titanite analyses cluster close to concordia at around 2.6 Ga, much younger than the zircon age and with no hint of earlier components within the grains. In summary, the titanites have been variably reset from original ages in the vicinity of 3.65-3.8 Ga. BSE images of some titanite grains imply that they were originally igneous and so later thermal events are most likely to have been culpable for the disturbance.
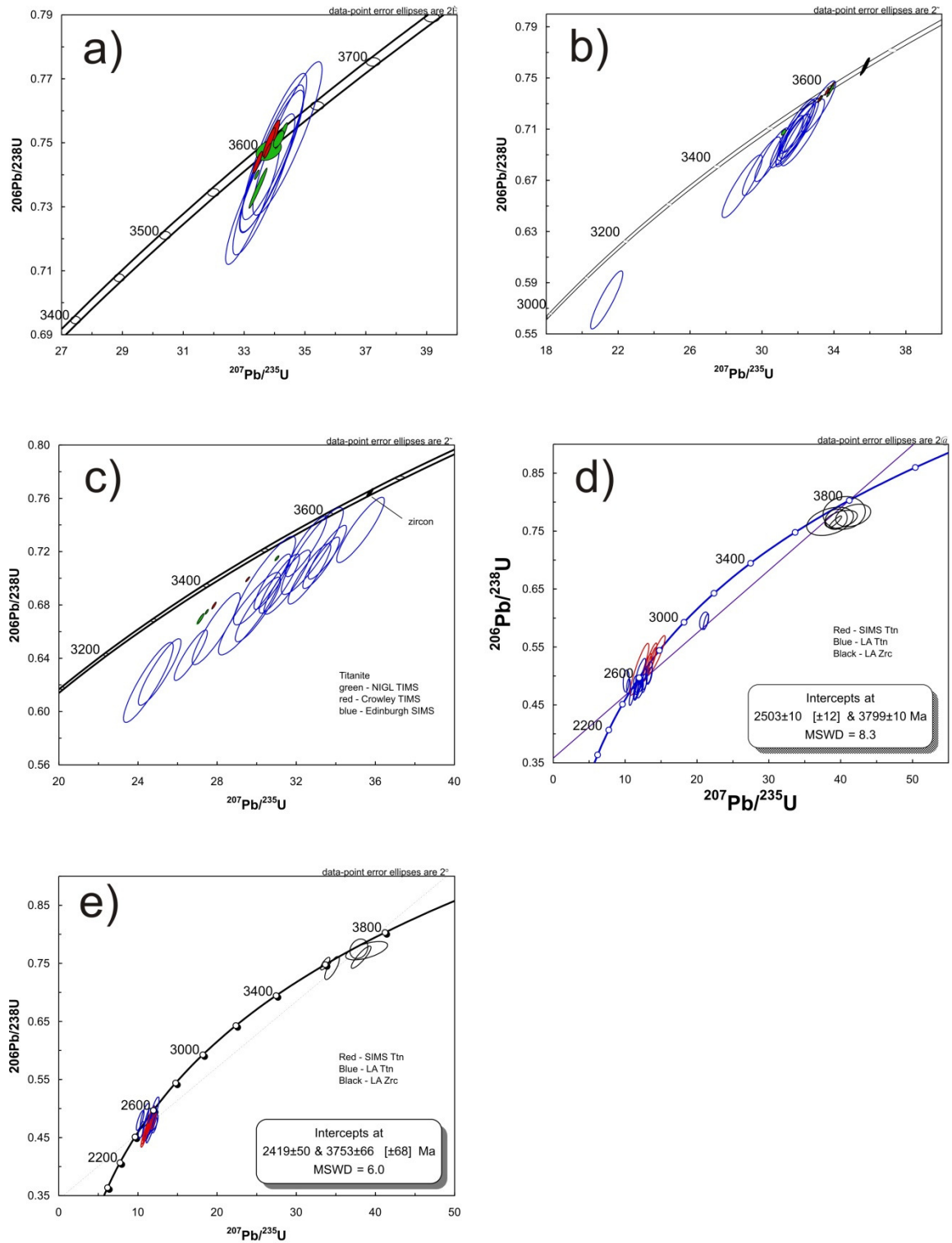
Fig. 1 U-Pb data collected in-situ by SIMS and LA-ICPMS and also by single grain ID-TIMS. a) JC130-99 b) JC133-99 c) JC200-00 d) SM/GR/98/2 e) SM/GR/00/2.

Oxygen isotopes from titanite and zircon pairs from two samples are available for comparison (Fig 2), unfortunately only from those strongly disturbed samples (SM/GR/98/2 and SM/GR/00/2). Given the similarity in closure temperature between Pb and O in titanite [6,7] these data must be treated with caution. For the other samples for which zircons were not available for analysis (JC130-99, JC133-99 and JC200-00) the titanite O analysis between

45

grains are reproducible within analytical uncertainty (Fig 3) and give the following $\delta^{18}O$ means and standard deviations: JC130-99 – 3.72 $\pm$0.26‰, JC133-99 – 4.34$\pm$0.28‰, JC200-00 – 3.69$\pm$0.33‰. Fractionation factors between zircon and titanite in magmatic systems indicate an offset of 1.2‰ to the lighter isotope in titanite [8] and, therefore, imply the following zircon $\delta^{18}O$ values: JC130-99 – 4.9‰, JC133-99 – 5.5‰, JC200-00 – 4.9‰. These vaules are within error of the accepted value of mantle zircon of 5.3$\pm$0.3‰ [9].

Summary

Titanites from gneissose rocks (tonalities and granodiorites) around the Isua Greenstone Belt of West Greenland have been variably reset due to later thermal events. However, in most cases it is convincing that the titanites were formed in the igneous host rock. In which case the zircon ages may be a better approximation of the time of crystallisation. For those samples where the titanites are little disturbed, the slightly younger ages could be due to cooling through their closure temperature later than zircon. In these cases the O isotopes are instructive. For those more greatly disturbed samples the O data should be treated with caution. In the more robust samples it is most likely that the precursor melts did not involve a component of sediments and so were either primary juvenile melts from the depleted mantle or reworked former juvenile melts. Future Nd isotope studies of these titanites should, therefore, give insight into the nature of the depleted mantle reservoir in the period 3.65-3.8 Ga.

References
[1] A.I.S. Kemp et al, Nature 439 (2006) 580-583.
[2] A.B. Pietranik et al, Geology 36 (2008) 875-878.
[3] J.L. Crowley et al, GSA Bull 114 (2002) 1311-1325.
[4] J.L. Crowley, Precam Res 126 (2003) 235-257.
[5] B.S. Kamber et al, Contrib Min Pet 145 (2003) 25-46.
[6] R.T. Pidgeon et al, Earth Planet Sci Lett 141 (1996) 187-198.
[7] X.Y. Zhang et al, Geochim Cosmochim Acta 71 (2007) 1563-1573.
[8] E.M. King et al, Geochim Cosmochim Acta 65 (2001) 3165-3175.
[9] J.W. Valley et al, Contrib Min Pet 133 (1998) 1-11.

SM/GR/98/2

a)

SM/GR/00/2

b)

4.34 ± 0.28   3.69 ± 0.33   3.72 ± 0.26
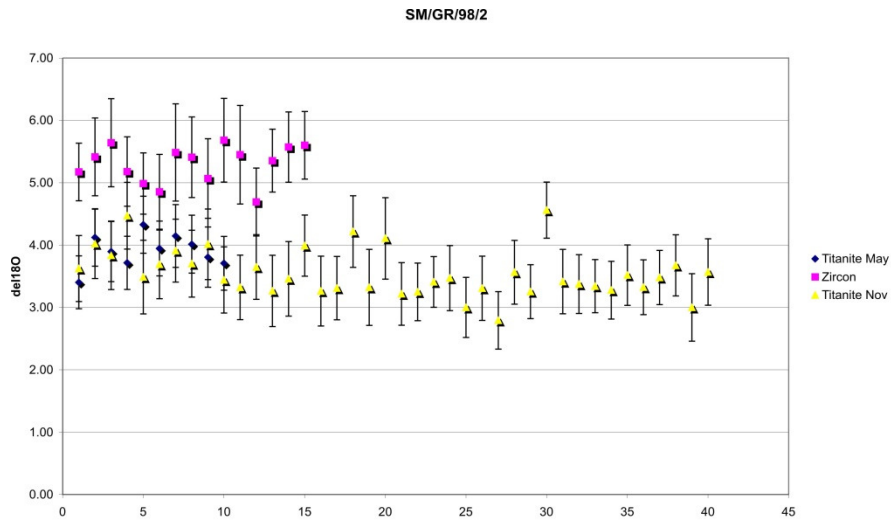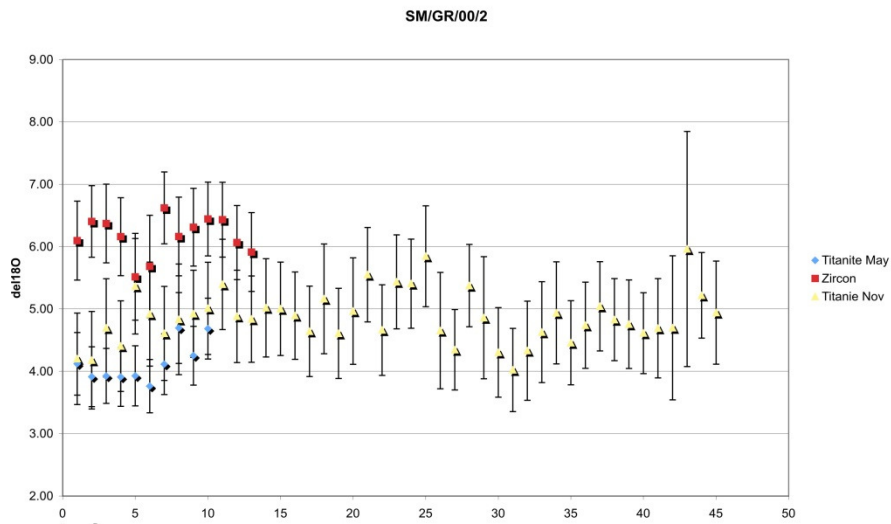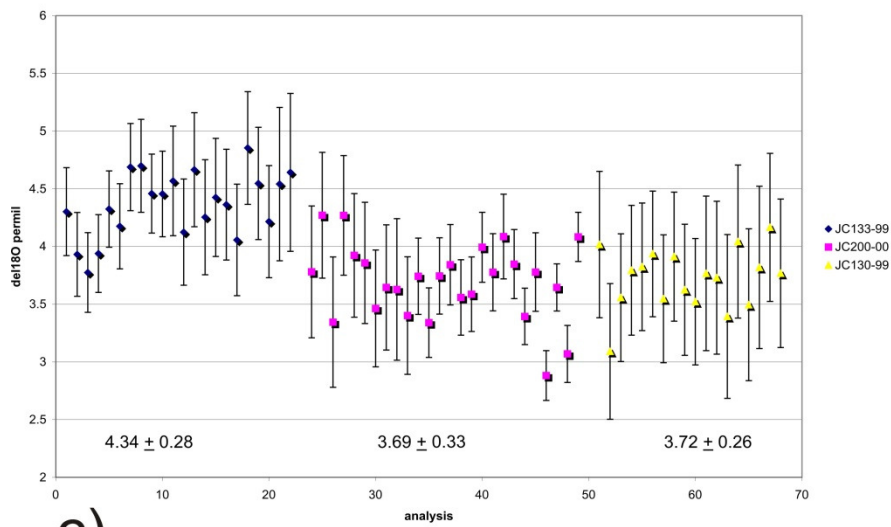
c)

Figure 2. Oxygen isotope analyses by SIMS. a) SM/GR/98/2 zircon and titanite b) SM/GR/00/2 zircon and titanite c) JC130-99, JC133-99 and JC200-00 titanite analyses for comparison.

Distribution of trace elements between zircon, garnet and melt: a key to understanding crustal events and processes

R.J.M. Taylor, S.L. Harley, R.W. Hinton & S. Elphick

[1]School of GeoSciences, University of Edinburgh, Edinburgh EH9 3JW, UK

Background

The interpretation of zircon age data in multiply-deformed and polymetamorphosed high grade terrains presents a significant problem in geochronology because the response of zircon to metamorphism is highly variable even on the microscale. The reliable interpretation of zircon age data must be founded upon detailed textural analysis coupled with in-situ microanalysis that yields independent chemical criteria for constraining the processes that have affected or controlled zircon behaviour. The distribution of REE and other trace elements between zircon and garnet in high-temperature crustal processes is being determined in this project, using both an empirical approach, based on in-situ analysis of zircon, garnet and co-existing phases in natural granulites and migmatites, and high-PT trace element doped experiments that yield zircon-granitic melt, garnet-melt and zircon-garnet-melt products. The distribution data are applied to evaluate the event significance of zircon ages in HT and UHT terranes, the responsiveness of zircon to post-peak mineral-melt reactions, and the relative importance of zircon recrystallisation versus new growth in metamorphism.

Results – Experimental Data

A series of experiments simulating granitic, crustal melts from pelitic rocks at high pressure and temperature are used to grow zircon and garnet in trace element equilibrium, to determine REE partition coefficients at a variety of relevant conditions.
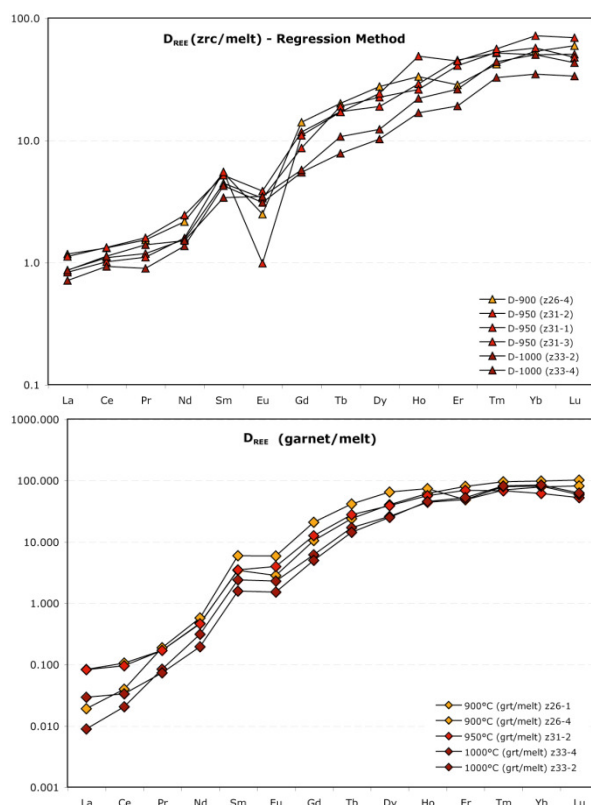
Fig.1 Edinburgh IMS-4f partitioning data for the REE between zircon and granitic melt in experimentally produced samples, at 7 kbar and 900-1000°C.

Fig.2. Edinburgh IMS-4f partitioning data for the REE between garnet and granitic melt in experimentally produced samples at 7 kbar and 900-1000°C.

REE values for experimentally produced zircon and garnet in granitic melt are obtained using the Edinburgh IMS 4f ion microprobe. Zircon grains are not large enough for single analyses, therefore a mixing line is used, ranging from clean melt to ~40% zircon, to extrapolate zircon REE concentrations.

D_{REE}(zrc/melt) data from garnet bearing experiments (fig.1) show a consistent pattern within the temperature range 900-1000°C with a positive slope in the M/HREE (D_{Gd} = 7-15, D_{Lu} = 40-80). This is very similar to the data from zircon-free experiments in similar melt compositions (Taylor et al., 2009).

D_{REE}(grt/melt) data from the same experimental runs show a consistent pattern within the temperature range 900-1000°C with D values <1 for the LREE and D values >1 for the middle to heavy REE. The D values plateau in the HREE with values of ~80-100

D_{REE}(zrc/grt) data for these runs is shown in Figure 3. While the D values for the LREE are imprecise and variable due to low concentrations in the garnet in particular, the middle to heavy REE produce consistent data with values approaching unity or slightly favouring garnet. DREE obtained for the MREE-HREE from Gd to Lu are in the range 0.4-1.5 for all temperatures examined, with the DREE pattern being flatter at 1000°C.. This experimental data can be matched to natural rock data, providing chemical criteria for showing zircon-garnet equilibrium in high-PT rocks, which is difficult to prove texturally.
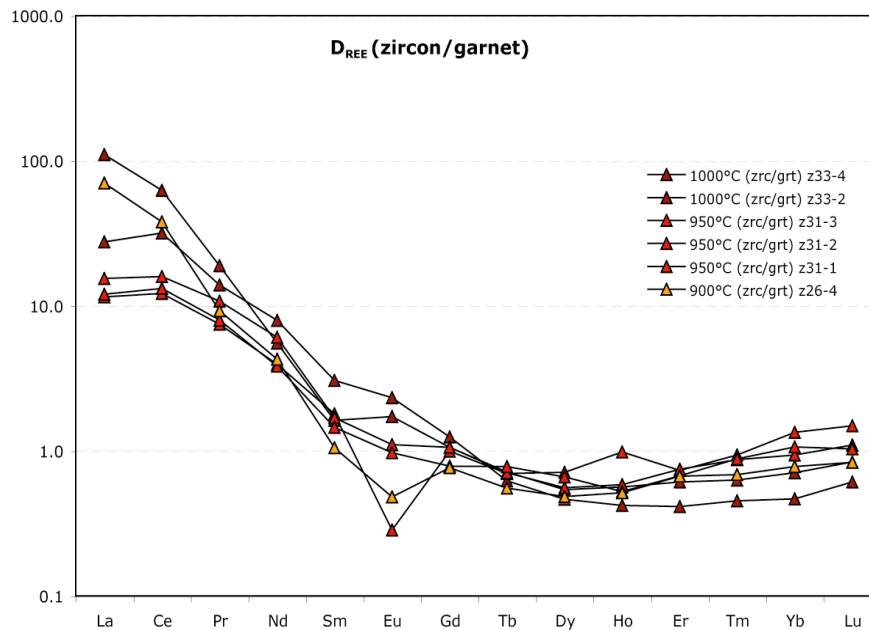
Fig.3 D_{REE}(zrc/grt) values for the experimental runs show a consistent dataset. LREE favour zircon, while the middle to heavy REE favour garnet or are close to unity. This data strongly supports the use of chemical criteria for the determination of equilibrium REE partitioning between, and therefore simultaneous growth of, zircon and garnet within high-grade metamorphic rocks.

Comparison with other studies

Application of the this data to published empirical studies show that the consistent D_{REE} (zircon/garnet) values for the middle to heavy REE are a powerful tool in showing the validity of examples from studies such as Harley et al (2001), Whitehouse and Platt (2003), Hokada and Harley (2004), Kelly and Harley (2005) and Baldwin and Brown (2008). Conversely, studies that have attributed steep DREE (zircon/garnet) patterns favouring zircon for the HREE such as Rubatto (2002), Hermann and Rubatto (2003) and Buick et al. (2006) may need to be re-evaluated in light of this new data.

A snapshot of mantle metasomatism

E.L. Tomlinson

Department of Earth Sciences, Royal Holloway University of London, Egham Hill, Egham, Surrey, TW20 0EX

Motivation for study

Trace element compositions of mantle xenoliths, xenocrysts and silicate inclusions in diamonds are frequently used as evidence for interaction with metasomatic fluids. Particular attention has been given to metasomatism by carbonate melts which are highly mobile and have strong LREE enrichment signatures. However, in no case is the metasomatic agent preserved and so its composition must always been inferred from partition coefficients. In this study we were able to directly compare the trace element composition of mantle silicates with their metasomatising fluid, using a unique set of fibrous diamonds from the Panda kimberlite (Canada) which contain both fluid inclusions (carbonate-H_2O-KCl and single-phase inclusions of garnet, olivine and clinopyroxene. The diamonds are lherzolitic, with a single eclogitic sample.

Method

SIMS was used to analyse a range of trace elements in clinopyroxene, garnet and olivine inclusions. The silicate inclusions are extremely small (typically <<15μm), precluding the use of LA-ICP-MS for accurate trace element determination. The trace element composition of the fluid was measured using LA-ICP-MS to bulk sample a multitude of micro-fluid inclusions.

Results and discussion

The silicate inclusions in our fibrous diamonds are comparable to published data for silicate inclusions in monocrystalline diamonds (Fig 1), suggesting that a similar fluid may be responsible for the growth of both fibrous and some monocrystalline diamonds. The inclusions in our fibrous diamonds are at the high end of the range of LREE concentrations reported in monocrystalline diamonds. The coexisting fluid is strongly enriched in LREE and LILE.
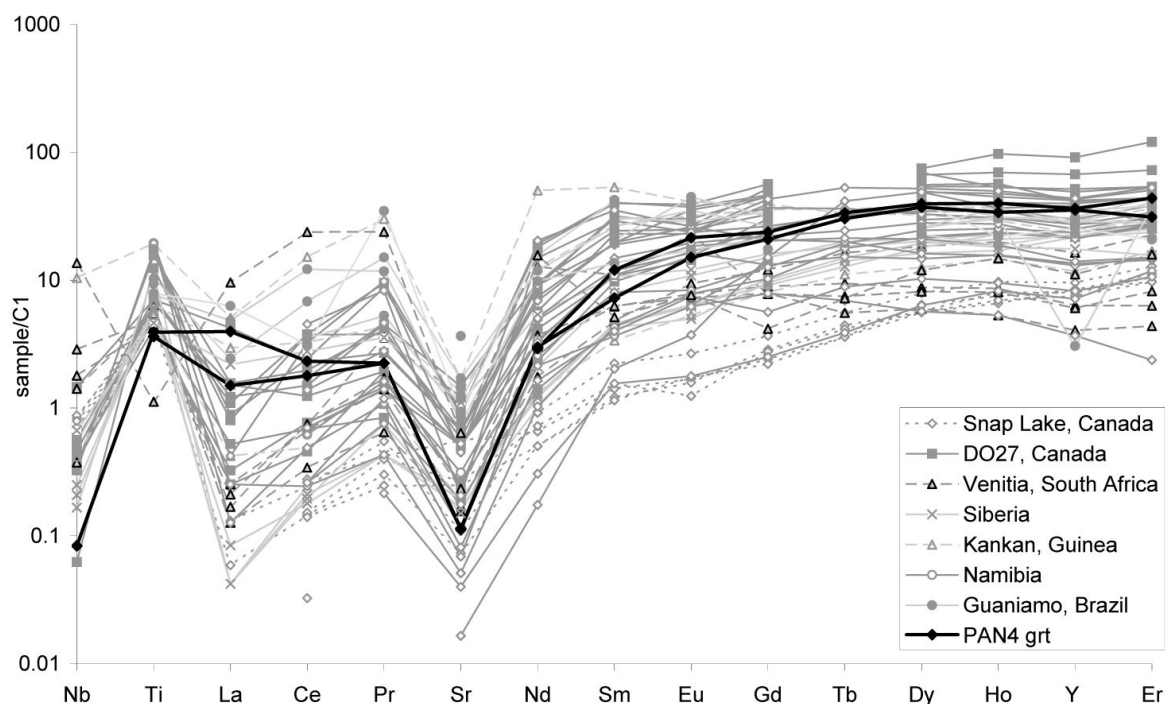
Fig. 1 Chondrite normalised trace element plot of two garnet inclusions in the eclogitic sample (PAN4), compared to published data for eclogitic garnet inclusions in monocrystalline diamonds.

We used the compositions of coexisting mineral and fluid inclusions in the Panda fibrous diamonds to calculate partition coefficients (D) between the carbonate–H_2O-KCl fluid and the clinopyroxene and garnet minerals. In general, there is good agreement between our partition coefficients calculated for the natural carbonate-diopside (lherzolitic) and carbonate-Na-rich clinopyroxene and carbonate-garnet (eclogitic) systems (Fig 2), and experimentally determined values. Because of the high variance of this natural system, these D values cannot be used to assess the controls on element partitioning. However, they do provide a unique snapshot of a natural system with which to compare experimentally derived D values.
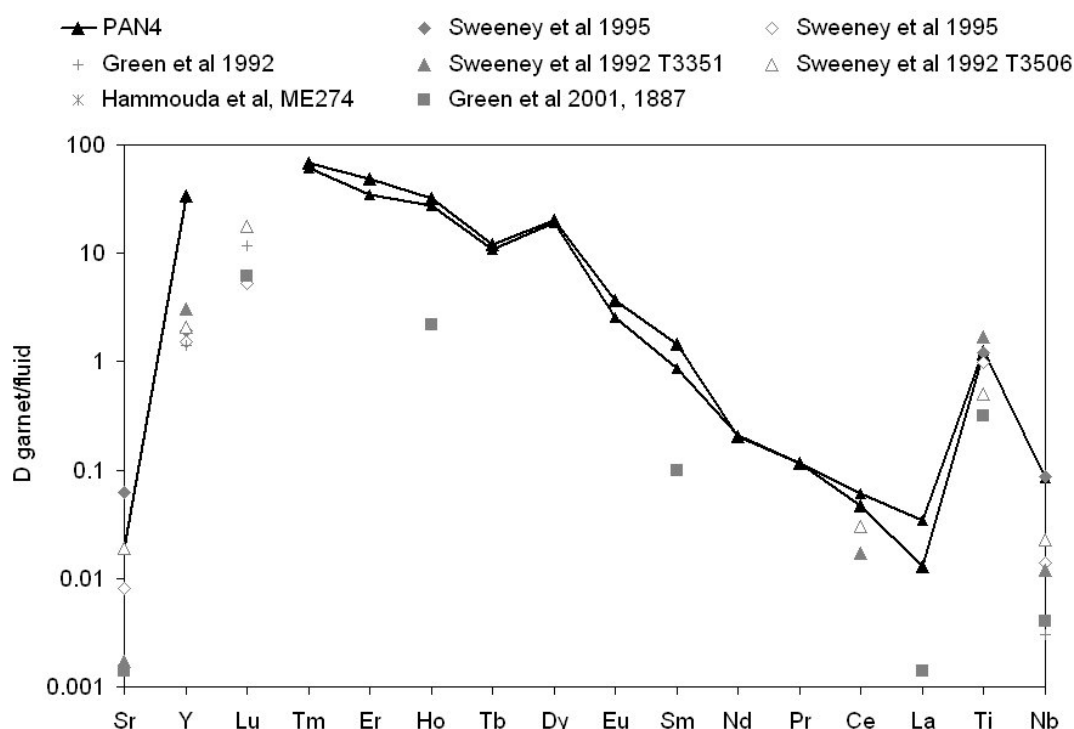
Fig. 2 Mineral-fluid partition coefficients ordered for eclogitic garnet in fibrous diamonds (PAN4) compared to experimentally determined garnet–carbonate partition coefficients.

References
[1] Aulbach, S., Stachel, T., Viljoen, K.S., Brey, G.P., Harris, J.W. Contrib. Mineral. Petrol. 143 (2002), 56–70.
[2] Davies, R.A., Griffin, W.L., O'Reilly, S.Y., Doyle, B.J. Lithos 77 (2004), 39–55.
[3] Kaminsky, F.V., Zakharchenko, O.D., Griffin, W.L., Channer, D.M., Khachatryan, G.K. Can. Mineral. 38 (2000)
[4] Promprated, P., Taylor, L.A., Anand, M., Floss, C., Sobolev, N.V., Pokhilenko, N.P., Lithos 77 (2004), 69–81.
[5] Stachel, T., Brey, G.P., Harris, J.W. Contrib. Mineral. Petrol. 140 (2000), 1–15.
[6] Stachel, T., Aulbach, S., Brey, G.P., Harris, J.W., Leost, I., Tappert, R., Viljoen, K.S. Lithos 77 (2004), 1–19.
[7] Taylor, L.A., Snyder, G.A., Crozaz, G., Sobolev, V.N., Yefimova, E.S., Sobolev, N.V. Earth Planet. Sci. Lett. 142 (1996), 535–551
[8] Green, T.H., Adam, J., Siel, S.H., 1992. Mineral. Petrol. 46 (3), 179–184.
[9] Hammouda, T., Moine, B.N., Devidal, J.L., Vincent, C. Physics of the Earth and Planetary Interiors, in Press
[10] Sweeney, R.J., Prozesky, V., Przybylowicz, W. Geochim. Cosmochim. Acta 59 (1995), 3671–3683
[11] Sweeney, R.J., Green, D.H., Sie, S.H. Earth Planet. Sci. Lett. 113 (1992), 1-14.

Plutonium Geochemistry of Meteorites

G. Turner[1], S.A. Crowther[1] & J.D. Gilmour[1]

[1]School of Earth, Atmospheric & Environmental Science, University of Manchester, Manchester M13 9PL

Introduction

The aims of this research project are to investigate the geochemical behaviour of plutonium in the Early Solar System and to constrain the Pu/U ratio, a parameter which has significance for theories of element synthesis and, by way of fissiogenic xenon isotopes, for theories of the evolution of the terrestrial mantle and atmosphere. The work is in two parts; a geochemical study of phosphates in primitive meteorites using the Edinburgh ion microprobe, and a study fissiogenic xenon isotopes in those phosphates using the Manchester resonance ionisation mass spectrometer (RELAX – Refrigerator Enhanced Laser Analyser for Xenon). The ion microprobe analyses of 44 phosphates and were carried successfully out in 2008. The xenon analyses are still pending, following a major upgrade to the laser laboratory and competition for instrument time from time critical international projects. The work carried out and projected xenon analyses are outlined below.

Ion Microprobe Analyses

Dr. Crowther made measurements on apatite and merrillite in 2 samples of Acapulco for the following elements: O, F, Na, Si, P, Cl, Ca, Sr, Y, Ba, all Lanthanides, Th and U. 10 merrillite and 15 apatite spots were analysed in "sample 1", and 7 merrillite and

12 apatite in "sample 2. Oxides were also measured in 3 spots, and a small number of measurements were made on non-phosphates for comparison.

The distinction between merrillite and apatite is clear in the attached compositional plots for chlorine and uranium. Apatite is rich in halogens including iodine, which makes it the preferred option for I-Xe dating, based on ^{129}Xe from the decay of now-extinct ^{129}I. It is also the major carrier of uranium.

Merrillite by contrast was the major repository for now-extinct ^{244}Pu. Attempts to estimate the ^{244}Pu abundance in the Early Solar System have been based on the supposed geochemical similarity between Pu and the light rare earths, more specifically Nd. Pu/Nd ratios combined with average Nd/U ratios have been used to infer the solar system Pu/U ratio 4.57 Gyr ago. The restricted range of Nd abundances in the merrillite contrasts with an order of magnitude range in the

apatite and one objective of the xenon analyses will be to see how variations in Nd/U correlate with Pu/U.

Xenon Analyses

As stated in the introduction, the Acapulco sections are still awaiting a slot on the analysis schedule of RELAX. An award from STFC, for the development of a second instrument for Kr analyses and an upgrade of the Xe instrument, RELAX, led to a major reorganisation of the laboratory in early 2008. An improved version of RELAX was subsequently put into operation, see [1]. Since then a major part of the analysis programme for RELAX has been the work associated with our commitments to the NASA Genesis mission to analyse the sun's atmosphere captured in silicon discs exposed to the solar wind over a period of 2 years in space. This, together with commitments to PhD student projects and some instrumental difficulties has prevented the analysis of the Acapulco phosphates. We shall attempt to remedy this situation in the coming months.
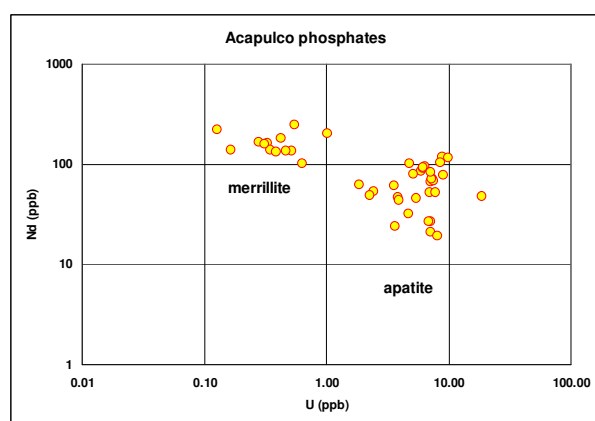
We plan first of all to carry out preliminary analyses on around six phosphates covering the full range shown in the ion probe data. The aim is to see to what extent we are able to determine the relative proportions of fissiogenic xenon from ^{238}U and ^{244}Pu. If Pu follows Nd it is likely that Pu will be difficult to distinguish in the apatites with the highest U/Nd ratios and U will be difficult to distinguish in the merrillites with the lowest U/Nd ratios. Based on the range in observed ion probe Nd/U ratios (see figure), we anticipate sufficient spread to find correlations between Nd/U and Pu/U if they exist. An alternative strategy for the merrillites which may be necessary if Pu/U ratios are too high will be to generate a component of fissiogenic xenon from neutron fission of ^{235}U. This would not be appropriate for the apatites (other than as a peripheral I-Xe dating exercise) and would not be carried out until most of the apatites had been analysed.

In conclusion we should add that the phosphate analyses require the highest sensitivity and in spite of the over long delays will benefit from the instrumental improvements related to the Genesis work.

References

[1] S.A. Crowther, R.K. Mohapatra, G. Turner, D.J. Blagburn, K. Kehm and J.D. Gilmour, Characteristics and applications of RELAX, an ultrasensitive resonance ionization mass spectrometer for xenon. J. Analytical Atomic Spectrometry (2008) 23:938-947.

[2] S.A. Crowther and J.D. Gilmour, Solar xenon in genesis silicon samples. Meteoritics and Planetary Sci. (2004) Suppl. 43:5236.

[3] J.D. Gilmour and S.A. Crowther, Solar xenon in genesis silicon. Geochim. Cosmochim. Acta (2008) 72:A310-A310.

Mineral/melt partitioning of trace elements between carbonate melt and deep mantle phases: constraints on the origin of ultra-deep mineral inclusions in diamonds

M. Walter[1], S. Keshav[2], G. Gudfinnsson[2], L. Armstrong[1], J. Tuff[1], and G. Bulanova[1]

1 Department of Earth Sciences, University of Bristol, Bristol BS* 1RJ, UK
2 Bayerisches Geoinstitut, Universita¨t Bayreuth, D-95440 Bayreuth, Germany

Introduction

Natural diamonds are transported from Earth's deep mantle to the surface, and some of these contain mineral inclusions formed in the mantle transition zone or lower mantle [1,2]. Our group has been investigating the origin of such ultradeep mineral inclusions in diamonds from the Juina area, Brazil. We find that the major and trace element geochemistry of majorite-garnet and rare, Ca-Ti-rich perovskite, indicate an origin as precipitates from carbonatitic melts in the deep upper mantle or transition zone [3]. This conclusion is based on trace element modelling indicating that the inclusions equilibrated with carbonatitic melt derived from eclogite. The trace element modelling that is critical to our inclusions is based on preliminary and incomplete partitioning data for minerals in equilibrium with carbonatitic melts at high pressures. In order to improve confidence in our models and to assess the possible effects of P, T and composition on partition coefficients, we have undertaken experiments to equilibrate mantle phases (e.g. pyroxene, garnet, perovskite) with carbonatitic melts. During our October 2008 session on the Cameca ims-4f ion probe at Edinburgh we analysed five experimental samples and obtained an excellent set of mineral/melt partitioning data for garnet (majorite), orthopyroxene, clinopyroxene, Ca-perovskite and forsterite. Here we briefly summarize some of the key findings, concentrating on the minerals most critical to our modelling, garnet and Ca-perovskite.

Results

Shown on Figure 1 are partition coefficients for garnet and majorite equilibrated with carbonatitic melts in experiments from 3.5 to 20 GPa. Surprisingly, we find very little effect on partitioning of
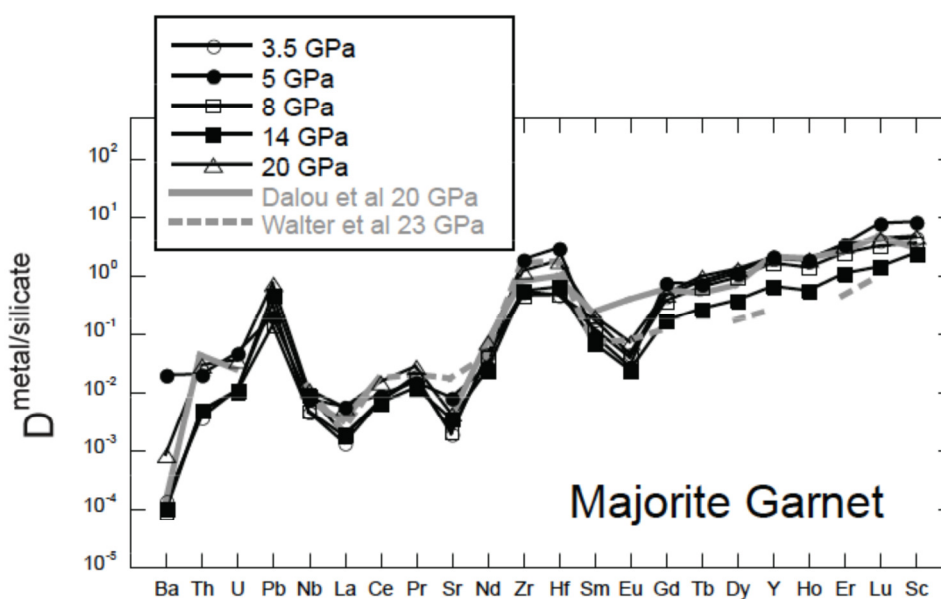
Fig. 1 Partition coefficients determined for garnet and majorite coexisiting with carbonatitic melts from 3.5 to 20 GPa. Also shown are data for majorite at 20 GPa (carbonatitic melt) [4] and at 23 GPa (silicate melt) [5].

pressure, melt or garnet composition. We find an exceptionally good match with recent data for majorite at 20 GPa, also equilibrated with a carbonatitic melt [4], and with data from [5] at 23 GPa in which majorite equilibrated with silicate melt. One exception is that our new data indicates an anomalously low partition coefficient for Eu relative to neighbouring REE. If real, this could provide a 'fingerprint' for garnet fractionation in the mantle. However, this feature has not been seen previously for garnet and we suspect an analytic artefact. Another interesting new feature is the relatively high partition coefficient for Pb relative to other LIL (Sr, Ba) and U and Th, and garnet fractionation would increase the U/Pb and Th/Pb ratio in a melt. Figure 2 shows partition coefficients determined for Ca-perovskite equilibrated with carbonatitic melt at 20 GPa. Again, we find very good agreement with recent data from [4].
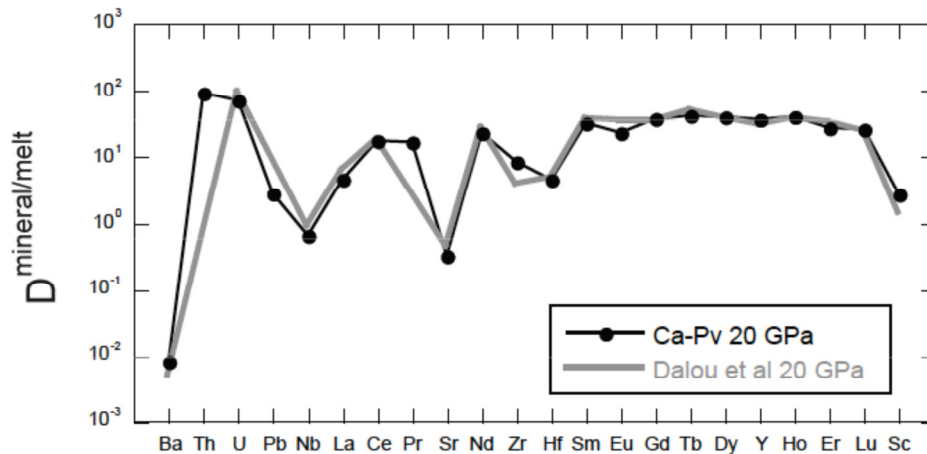
Fig. 2 Partition coefficients determined for Ca-perovskite coexisting with carbonatitic melts from at 20 GPa. Shown for comparison is recent data from [4] at 20 GPa.

We are using these data to model fractionation of Ca-perovskite and garnet from primary carbonatitic melts derived in the deep mantle. Figure 3 shows an example of a calculated fractionated liquid (crystallization of Ca-Pv, garnet and ilmenite) that matches very closely to the composition of liquids calculated to coexist with majorite garnet inclusions in diamonds from Juina (Bulanova et al., in prep).
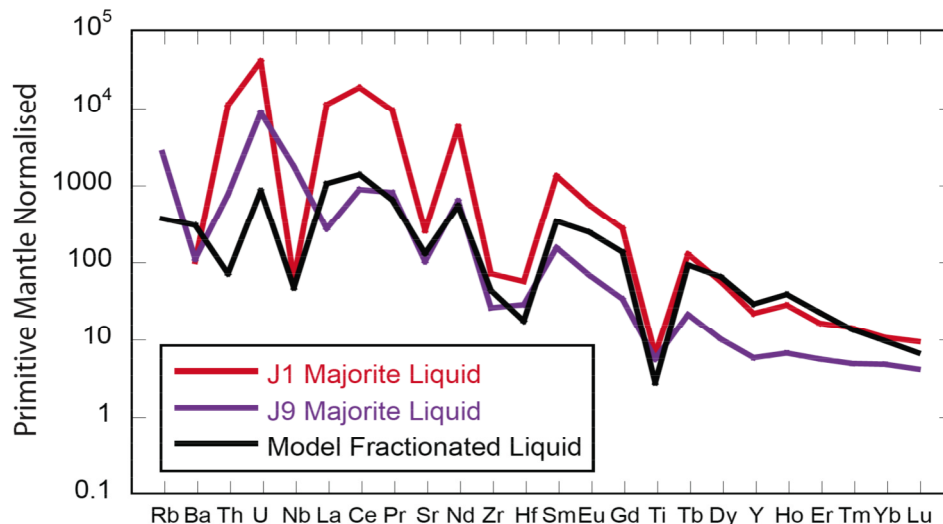
Fig.3 Calculated trace element composition of melts that could coexist with majoritic garnet inclusions in diamonds J1 (red line) and J9 (purple line). Also shown is a model fractionated liquid (black line) that is calculated assuming 40% fractional crystallization each of majoritic garnet + Ca-Pv and an HFSE-rich phase (e.g. ilmenite) from an initial primary carbonatite from eclogite (Bulanova et al., in prep).

References
[1] Harris, J (1992). In: Field, J.E., (Ed), Academic Press, London, 345-393.
[2] Harte and Harris (1994), Mineralogical Magazine, 58A, 384-385.
[3] Walter et al (2008), Nature, 454, 622-626.
[4] Dalou et al (2008), Geochim. Cosmochim. Acta, 73, 239-255.
[5] Walter et al (2004, Geochim. Cosmochim. Acta, 68, 4267-4284.